Compression Creep of Filamentary Composites

by

D. L. Graesser, Research Assistant
M. E. Tuttle, Assistant Professor

Department of Mechanical Engineering, FU-10
University of Washington
Seattle, WA 98195

Prepared For:
NASA-Langley Research Center
Grant No. NAG-1-621
University Contract No. 62-7541
Mr. J. D. Whitcomb, Project Monitor

March1988

University of Washington

COMPRESSION CREEP OF FILAMENTARY COMPOSITES

ABSTRACT

Axial and transverse strain fields induced in composite laminates subjected to compressive creep loading were compared for several types of laminate layups. Unidirectional graphite/epoxy as well as multi-directional graphite/epoxy and graphite/PEEK layups were studied. Specimens with and without holes were tested. The specimens were subjected to compressive creep loading for a 10 hour period. All tests were conducted at room temperature and ambient humidities.

In-plane displacements were measured using moiré interferometry. A computer based data reduction scheme was developed which reduces the whole-field displacement fields obtained using moiré to whole-field strain contour maps. This approach proved to be an ideal method of displaying the data obtained using moiré interferometry.

Only slight viscoelastic response was observed in matrix-dominated laminates, except for one test in which catastrophic specimen failure occurred after a 16-hr period. In this latter case the specimen response was a complex combination of both viscoelastic and fracture mechanisms. No viscoelastic effects were observed for fiber-dominated laminates over the 10 hour creep time used in this study. The experimental results for specimens with holes were compared with results obtained using a finite-element analysis. The

comparison between experiment and theory was generally good. Overall strain distributions were very well predicted. The finite element analysis typically predicted slightly higher strains values at the edge of the hole, and slightly lower strains values at positions removed from the hole, than were observed experimentally. It is hypothesized that these discrepancies are due to nonlinear material behavior at the hole edge, which were not accounted for during the finite-element analysis.

TABLE OF CONTENTS

APPENDIX A

LIST OF FIGURES

LIST OF TABLES

ACKNOWLEDGEMENTS

The authors wish to thank the many individuals who have helped make this work possible. Financial support was provided through NASA-Langley Grant No. NAG-1-621. Mr. John D. Whitcomb has acted as Project Monitor. Sincere thanks are extended to Mr. Whitcomb for his encouragement and many helpful suggestions. The technical advice and insight of Prof. Ken Y. Lin is gratefully acknowledged. Thanks are extended to Profs. Minoru Taya and Colin H. Daly who edited the draft version of this report. Thanks is given to Mr. Raymond J. Klein for his technical advice regarding the use of the moiré interferometry and loading system. Mr. Russ McGuire of Boeing Commercial Airplane Company provided the Gr/Ep panels used in the study. Profs. Dan Post and Robert Czarnek of Virginia Tech, Prof. Jon Epstein of Georgia Tech, and Dr. Vance Deason of Idaho National Laboratories all made valuable contributions to this study. And finally sincerest thanks goes to Mr. Mahyar S. Dadkhah and Visiting Prof. F.X. Wang of UW for their technical advice and assistance on all parts of this project.

INTRODUCTION

The advent of fiber-reinforced composites materials has been termed the "biggest technical revolution since the jet engine."[1] Advanced polymeric composite materials exhibit high strength-to-weight and stiffness-to-weight ratios. These qualities make composite materials extremely useful in applications where high performance and weight savings are important. Aircraft and spacecraft are typical weight-sensitive structures in which composite materials are cost effective. Composite materials usually exhibit the best qualities of their constituent components and often some desirable qualities that neither component possesses separately. Modern composites offer a dramatic improvement in mechanical/thermal capabilities, when compared to conventional monolithic materials, including an increase in; strength, stiffness, corrosion resistance, wear resistance, attractiveness, weight, fatigue life, thermal conductivity and acoustical insulation.[1]

Composites made from strong continuous fibers embedded in a relatively weak matrix material exhibit anisotropic behavior when subjected to loading. Hence the mechanical and thermal behavior of composites is often much different than the behavior exhibited by familiar isotropic materials such as steel or aluminum. A considerable study of composites has focused on the response to tensile loading. Significantly less study has been devoted to the behavior of composites in compression. The research described herein was an investigation of the response of composite laminates

to uniaxial compressive loading, and should contribute towards a greater understanding of the compressive behavior of composites.

Polymeric composites exhibit viscoelastic behavior which is more pronounced than that exhibited by traditional engineering materials. These effects, in general, become more evident at elevated temperatures, although significant viscoelastic behavior also occurs at room temperatures over long time periods. Exposure to various plasticizers such as moisture, jet fuel, or gasoline can also result in an increase in viscoelastic behavior. The expected service life of composite structures can be on the order of tens of years, and therefore viscoelastic response may result in delayed failure or excessive deflections after some years in service. Consequently a clear understanding of the nature and magnitude of this viscoelastic behavior is important with the increasing use of composites as substitutes for traditional materials.

A study of composites in compression was initiated at the University of Washington in 1986. The study was supported through a two-year grant provided by the Fatigue and Fracture Branch of the NASA-Langley Research Center. The program can be roughly divided into two complementary efforts, one involving an analytic (i.e., finite-element) analysis and the second involving an experimental analysis. The present report describes the experimental efforts which have been performed during the second year of the UW/NASA-Langley study. Comparisons between experimental

results the finite-element analyses are presented where appropriate.

The experimental portion of the study has involved the application of compressive creep loads to composite laminates. All tests have been performed at room temperatures and ambient humidity conditions. Two distinct material systems have been investigated: Hercules graphite-epoxy (G/E) IM7-8551 and Imperial Chemical Industries (ICI) graphite-PEEK (G/P) APC-2. Several different laminate layups and specimen geometries have been used.

One unique aspect of the experimental analyses has been the use of moiré interferometry to measure in-plane surface displacements. Moiré interferometry is a state-of-the-art optical method which provides whole-field displacement contours. The technique was developed during the late 1970s' and early 1980s'[2][3]. Moiré interferometry has since been used extensively to study the behavior of composites[4][5][6] as well as other structural materials[7][8][9][10][11]. However, to the authors' knowledge this is the first time moiré interferometry has been used under creep conditions.

OBJECTIVES

The experimental efforts performed during the first year of the study have been previously described in several publications by Klein and Tuttle[12][13][14]. Klein's study was devoted primarily to the design and development of the experimental apparatus required. Specifically, Klein developed a compressive loading fixture (required to apply a uniaxial compressive creep load to the composite specimen) and a laser-based optical system (used to measure the resulting surface displacements using moiré interferometry). The experimental system was successfully used by Klein to obtain moiré patterns for a relatively limited number of tests. In-plane strains were then calculated using an essentially graphical procedure. This technique was tedious and time-consuming. Furthermore, the data reduction scheme only allowed for calculation of strains along discrete lines or "slices" through the moiré image[12]. Hence, whole-field strain measurements were not obtained. Klein recommended that an alternate data reduction scheme be developed to automate the data reduction process, hopefully resulting in a more accurate calculation of strain levels as well as whole-field strain contours.

The present report describes the experimental efforts performed during the second year of the UW/NASA-Langley study. An expanded series of tests have been performed, and a more sophisticated data reduction scheme has been developed. The specific goals of the present study were as follows:

- To perform creep tests using unidirectional $[0]_{48}$ and $[90]_{48}$ laminates. These data would allow calculation of the engineering moduli E_{11}, E_{22}, n_{12}, and would also indicate the extremes of viscoelastic behavior to be expected from a "fiber-dominated" laminate layup versus a "matrix-dominated" laminate layup.
- To perform creep tests using a multiple-angle laminate whose behavior was expected to be "fiber-dominated"; the layup selected was $[0/45/0/-45]_{6s}$.
- To perform creep tests using a multiple-angle laminate whose behavior was expected to be "matrix-dominated"; the layup selected was $[90/-45/90/45]_{6s}$.
- To develop a computer-based data reduction scheme which would provide whole-field strain contours based upon moiré fringe patterns.

TESTING EQUIPMENT

Compression Fixture

As previously mentioned, the compression fixture used in this study has been fully described in refs [12-14]. The fixture is a modification of the "end-loaded coupon" fixture, originally proposed by Clark and Lisagor[15]. The UW version of this device is shown schematically in Figure1. The fixture was designed to satisfy the following criteria:

The fixture must:

1) Apply compressive loading to the specimen using either:
   a) A SATEC lever arm creep frame, or
   b) A Tinius Olsen Universal testing frame.
2) Insure that the applied load is "purely" uniaxial compression, applied through the centroid of the specimen cross-section.
3) Rigidly constrain the specimen to prevent rigid body motion.
4) Allow for easy inclusion in a moiré interferometry optical system.

Extensive fixture verification was conducted by Klein[12] , through the use of strain gaged aluminum test specimens. It was found that the fixture does indeed produce a nearly uniaxial compressive load. The bending moments which are (inadvertently) induced result in bending strains whose magnitudes are typically less than 5% of the total axial strains.[12] Hence, the effects of bending have been

ignored during the present study, i.e. it is assumed in all cases that the specimens are subjected to purely uniaxial compressive loading.

Moiré Fixture

The moiré interferometry fixture used in this research has been described in detail in ref [12-14]. The fixture uses a pair of two intersecting beams to produce a virtual reference grating. The virtual reference grating, in conjunction with a diffraction grating bonded to the specimen, results in a moiré pattern. A sketch of the system is shown in Figure 2. A single 152 mm (6 inch) diameter laser beam is incident upon the fixture and mirrors A-D. These mirrors separate the incoming beam into four separate beams, which are then directed toward mirrors E-H. The second set of mirrors direct the beams of light to the specimen at an angle of 17.98°. This angle will produce a virtual reference grating with a frequency of 1200 l/mm, when used with laser light produced by the argon-ion laser used in this study, i.e., light with a wavelength of 514.4 nm[2][16][17]. Mirrors E-H can be rotated in two out-of-plane directions, so as to precisely adjust the frequency and orientation of the virtual reference gratings. Mirrors A & C are used to create a virtual reference grating for use in producing moiré patterns associated with "x"-displacements. Similarly, mirrors B & D are used to produce a virtual reference grating in the "y"-direction[12][18].

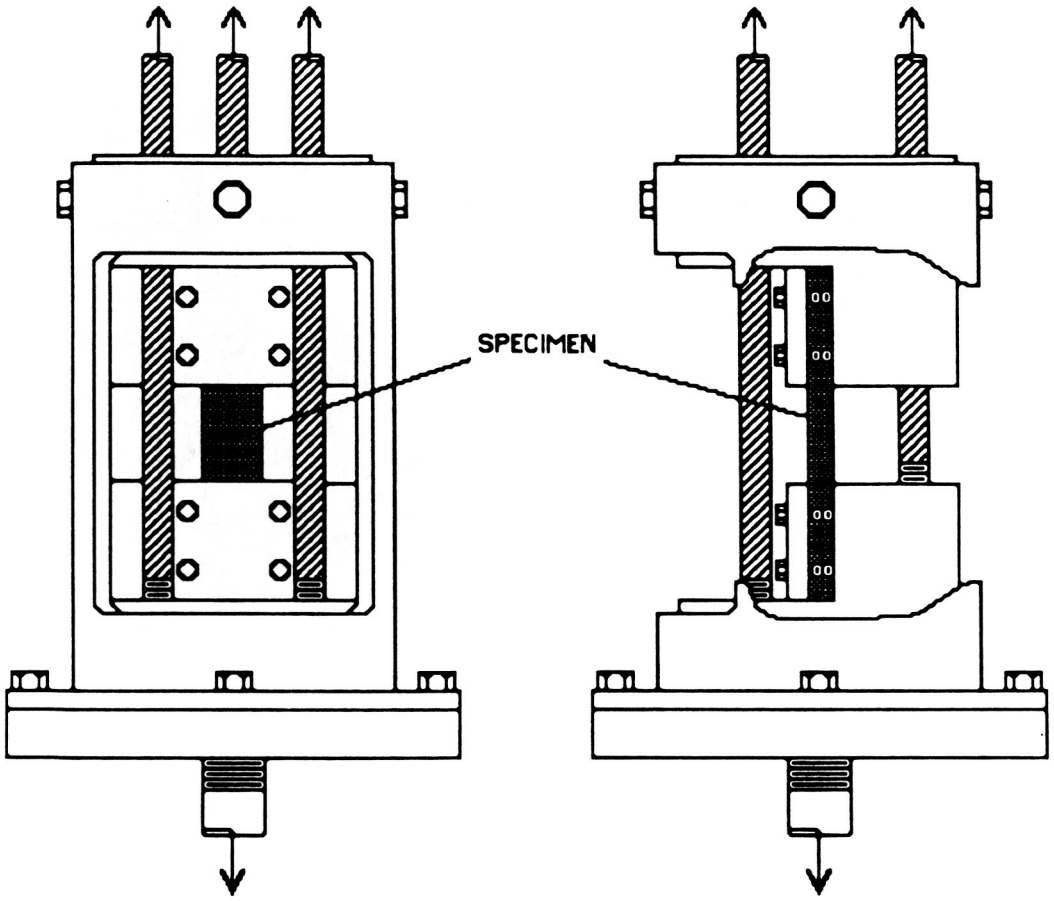

Figure 1: Compression Fixture in the SATEC Creep Frame. (Schematic)

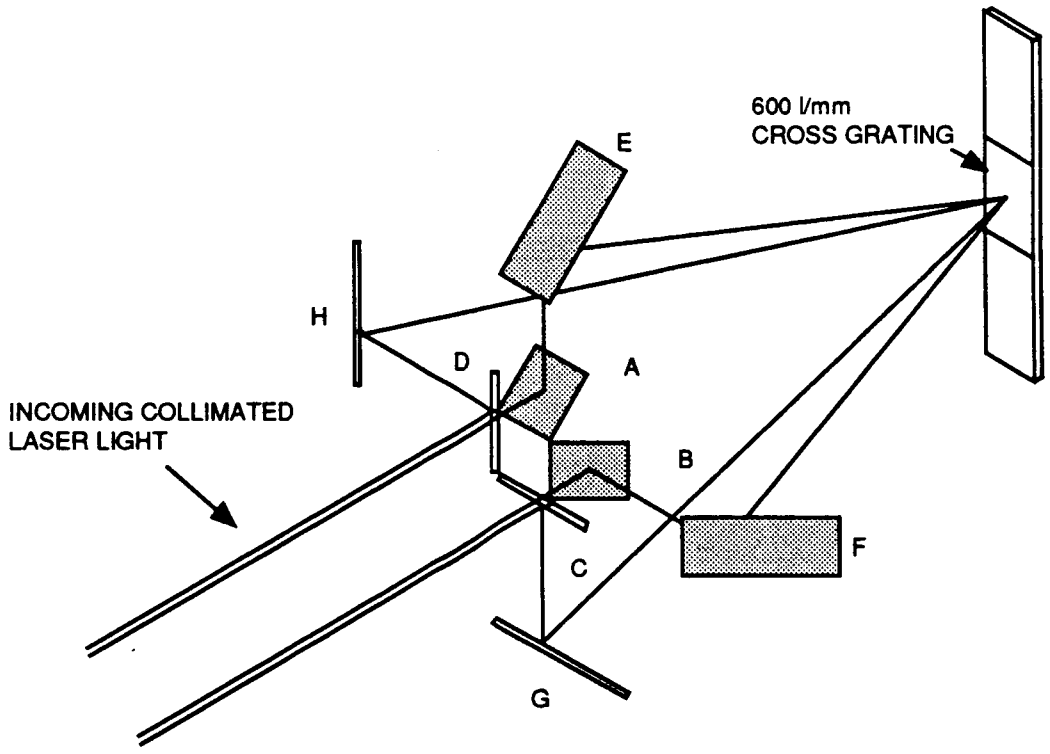

Figure 2: Mirror Arrangement for the Moiré Fixture. (Schematic)

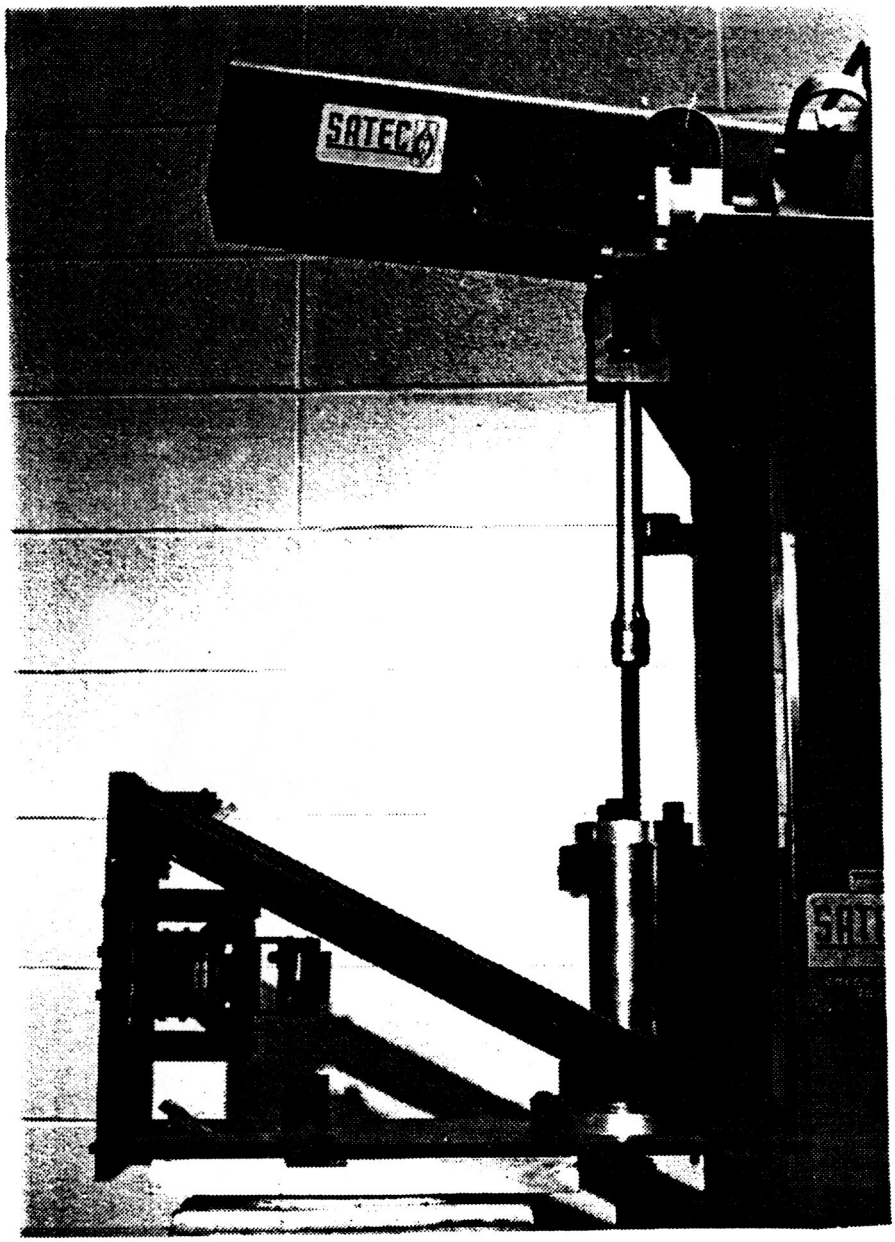

Figure 3: Moiré and Compression Fixture in the SATEC Creep Frame.

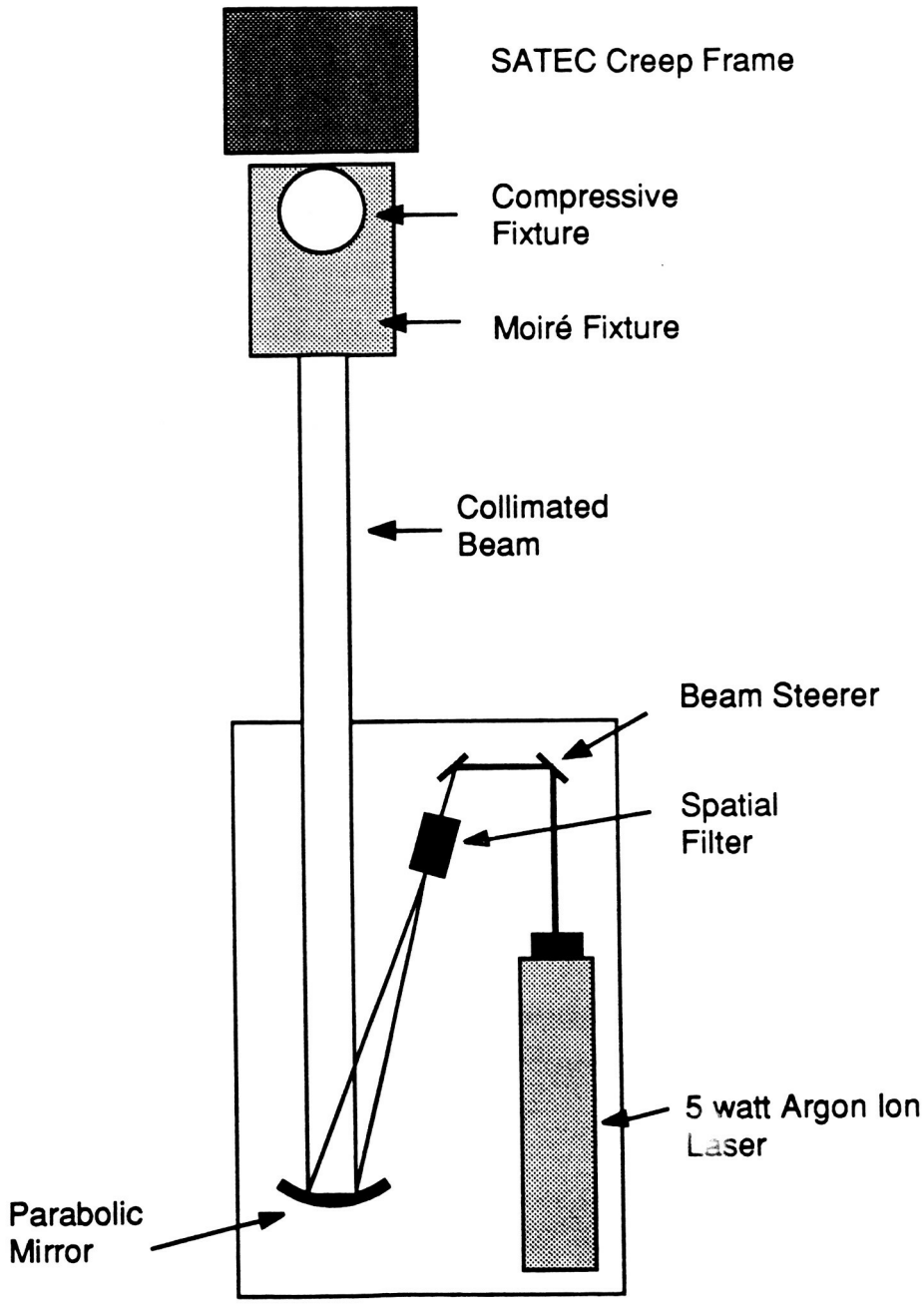

Figure 4: Moiré Optical Set-up.

Testing Frames

A SATEC Model G creep tester was used in all moiré tests. This machine utilizes a dead weight lever arm system, with a maximum tensile load of 88,960 N (20,000 lbs). Figure 3 shows the moiré and loading fixture mounted in the Satec creep frame.

A Tinius Olsen universal load frame was used to determine the static ultimate compressive strength of the composite specimens. The Tinius Olsen can apply a maximum compressive load of 266,880 N (60,000 lbs).

Laser and Optics

A Spectra Physics Series 2000 Argon Ion Laser, Model No. 2020-05, was used to produce a monochromatic light beam with a wavelength of 514.4 nm. The laser is capable of producing a laser beam with an intensity of up to 5 W, however only 200-300 mW were necessary to properly expose the photographic film used in this study.

The light beam emanating from the laser head is expanded to form a 152 mm (6 in) dia beam of collimated light. The optical system used to expand and collimate the beam is shown schematically in Figure 4. The laser beam is first directed to a 10X 25 μm spatial filter using several beam steering mirrors. The light which passes through the spatial filter is diffracted (i.e. "bent"), causing the beam to expand in the cone-shaped envelope indicated in Figure 4. This expanding beam of light then impinges

upon a 152 mm dia parabolic mirror, which in turn reflects a collimated beam of light with the required 152 mm diameter. The parabolic mirror is adjusted so as to direct the reflected beam towards the moiré fixture, providing the "incoming light beam" previously shown in Figure 2.

Camera and Film

A Cannon 35 mm camera, (base only), was used to photograph the moiré fringe patterns, using shutter speeds ranging from 1/500 to 1/2000 secs. Since the diffraction gratings used in this study had dimensions of 25.4 x 25.4 mm (1 x 1 in) the actual area of the moiré pattern emanating from the specimen surface was 645 mm^2 (1 in^2). A f1.4 lens was used to condense and focus the moiré pattern on the 35 mm film plane. Kodak Tri-X Pan, black and white film was used to record the pattern. The film was processed according to the manufacturers recommended procedure. Prints of the moiré patterns were produced using Kodak Poly Contrast Rapid II RC paper. Poly Contrast is a multi-contrast paper. A no. 4 contrast filter was used to produce satisfactory contrast. Standard development procedures were used to develop the prints.

Specimen Preparation

Nominal specimen dimensions were 152.4 mm (6 in) long, 25.4 mm (1 in) wide and 6.35 mm (.25 in) thick. Approximately 51 mm (2 in) of either end of the specimen is constrained within the end-loaded-coupon test fixture (see Figure 1), and hence the

unsupported gage length was nominally 51 mm (2 in). The Boeing Commercial Airplane Company supplied a IM6 graphite-epoxy $[0]_{48}$ unidirectional panel and a IM6 graphite-epoxy $[0/45/0/-45]_{6s}$ panel. Imperial Chemical Industries (ICI) supplied an APC-2 graphite-PEEK $[45/0/-45/90]_{6s}$ panel. Specimens were cut from these three panels using a diamond coated abrasive disk. Holes (if required) were drilled using a carbide tipped drill.

Moiré grating molds, used to produce the specimen gratings, were prepared as described by Basehore and Post[19]. The specimen grating frequency was 600 l/mm. Crossed-gratings were used. Specimen preparation requires bonding the diffraction grating to the specimen surface. Specimen surface preparation is similar to techniques used when bonding resistance foil strain gages[20]. The moiré grating mold is coated with a 500 Å layer of aluminum using a vapor deposition system. Either Micro Measurement PC-10 or PC-6 adhesive was used to bond the aluminum coating to the specimen surface. The adhesive is allowed to cure for 24 hours and excess epoxy is removed from the edges of the grating using a razor blade. The grating mold is then gently pried up, leaving the reflective diffraction grating bonded to the specimen surface.

Test Matrix

The selection of the laminate layup was conducted with the following in mind.

1) A determination of the fundamental engineering moduli E_1, E_2, n_{12} and n_{21} was of interest. This information could be found by analysis of unidirectional specimens, both $[0]_{48}$ and $[90]_{48}$.
2) Viscoelastic properties of multi-angle composite laminates were a concern. Miyano, Kanemitsu, Kunio and Kuhn[21] have reported that some matrix dominated layups exhibit viscoelastic tendencies at room temperatures. Therefore, both a matrix dominated layup, $[90/-45/90/45]_{6s}$, as well as a fiber dominated layup, $[0/45/0/-45]_{6s}$, were investigated during this study.

The $[0]_{48}$ and $[90]_{48}$ specimens were cut from a single 48-ply "parent" panel. The $[0/45/0/-45]_{6s}$ and $[90/-45/90/45]_{6s}$ specimens were cut from a single $[0/45/0/-45]_{6s}$ parent panel.

Selection of Creep Stress Levels

The quasi-static ultimate strength of each specimen was determined using specimens mounted in the Tinius-Olsen test frame. The ultimate strength tests are summarized in Table 1. The "specimen type" indicates both the material system and laminate layup (i.e., unidirectional or multi-angle laminate) for each specimen. The "specimen geometry" indicates the specimen hole diameter, if applicable. Each specimen was loaded in compression at a constant crosshead rate of 0.025 in/min. Audible cracking was heard throughout each test, up to and including specimen failure. The load at which complete catastrophic failure occurred was

recorded during each test and is listed as the "major failure load" in Table 1. The "major failure stress" was then calculated as the failure load divided by the net-cross sectional area, i.e., $S_{fail} = P/A_{net}$. For specimens with holes a higher stress actually existed at failure, due to the stress-concentrating effect of the hole. No attempt was made to determine the actual maximum stress level induced in these specimens at failure.

Once the ultimate strength of each specimen had been determined it was possible to select an appropriate creep stress level. The original intention was to test each specimen at a creep stress equal to 90% of the ultimate strength. However, in several tests it was found that a stress level of this magnitude resulted in moiré fringe patterns which were so dense that individual fringes could not be identified. This was especially true of the "matrix-dominated" layups. Consequently creep stress levels were adjusted for each specimen so as to result in a moiré pattern exhibiting a large number of fringes which could still be adequately interpreted.

The creep stress levels used during the moiré tests are summarized in Table 2. The "load applied" for each specimen type is indicated in the table. The corresponding "stress applied" equals the applied load divided by the net cross section. Again note that the concentrating effects of the holes are not accounted for in the value given for the applied stress. Finally, the "% of ultimate" relates the

creep stress level to the specimen ultimate strength, as previously presented in Table 1.

TABLE 1 - ULTIMATE STRENGTH

Test #	Specimen type*	Specimen Geometry	Major Failure Load	Major Failure Stress
1	A	6.35 mm dia Hole	77,800 N	643 MPa
2	A	No Hole	102,300 N**	634 MPa
3	B	6.35 mm dia Hole	64,500 N	533 MPa
4	B	No Hole	102,300 N**	634 MPa
5	C	6.35 mm dia Hole	24,500 N	202 MPa
6	C	No Hole	33,400 N	207 MPa
7	D	6.35 mm dia Hole	41,400 N	342 MPa
8	D	No Hole	65,500 N	400 MPa
9	E	1.58 mm dia Hole	65,600 N	434 MPa
10	E	3.17 mm dia Hole	62,300 N	441 MPa
11	E	6.35 mm dia Hole	40,000 N	331 MPa
12	E	9.52 mm dia Hole	37,900 N	375 MPa

* Specimen types are defined as follows:

Type A IM7-8551 graphite-epoxy $[0]_{48}$
Type B IM7-8551 graphite-epoxy $[0/45/0/-45]_{6s}$
Type C IM7-8551 graphite-epoxy $[90]_{48}$
Type D IM7-8551 graphite-epoxy $[90/-45/90/45]_{6s}$
Type E APC-2 graphite-PEEK $[45/0/-45/90]_{6s}$

** The type A and B specimens with no hole had premature failures in the grip area.

TABLE 2 - TEST MATRIX

Test #	Specimen type*	Specimen Geometry	Load Applied	Stress Applied	% of Ultimate
1	A	6.35 mm dia Hole	40,000 N	330 MPa	62%
2	A	No Hole	80,100 N	496 MPa	78%
3	B	6.35 mm dia Hole	50,700 N	419 MPa	78%
4	B	No Hole	66,700 N	413 MPa	65%
5	C	6.35 mm dia Hole	8,000 N	66 MPa	33%
6	C	No Hole	5,300 N	33 MPa	16%
7	D	6.35 mm dia Hole	18,700 N	154 MPa	45%
8	D	6.35 mm dia Hole	37,400 N	308 MPa	90%
9	D	No Hole	18,700 N	115 MPa	29%
10	E	1.58 mm dia Hole	50,700 N	335 MPa	77%
11	E	3.17 mm dia Hole	42,700 N	302 MPa	69%
12	E	6.35 mm dia Hole	37,400 N	308 MPa	93%
13	E	9.52 mm dia Hole	24,000 N	238 MPa	63%

* The specimen types are listed in Table 1.

CALCULATION OF STRAIN FROM MOIRE FRINGES

Moiré fringe patterns represent lines of constant surface displacement. Although in some cases measured dispplacements are used directly[22], normally the strain fields induced by external loading are of greater interest than the associated displacement fields. Hence, conversion of the displacements revealed by a moiré fringe pattern to the corresponding strain field is usually desired. The moiré patterns recorded during the present study were reduced to in-plane strain fields. The various techniques which have been used to perform this conversion can be roughly grouped into two categories; "mechanical differentiation"[17] and the "displacement-field approach"[23]. The data reduction scheme used in the present study is based upon the displacement-field approach; both categories will be briefly explained below.

Data Reduction by Mechanical Differentiation

One category of reducing moiré patterns to the corresponding strain fields includes methods based upon "mechanical differentiation" (also known as "moiré of moiré", "super moiré", or "second-order moiré" -- the reader is warned that these terms are not uniformly applied, and different authors may use the same term to refer to a fundamentally different experimental technique). One way of performing mechanical differentiation is through the use of two identical transparencies (e.g., photographic negatives) of a moiré fringe pattern. The two transparencies are initially exactly aligned, such that the original fringe pattern is observed. One of the

transparencies is then shifted with respect to the second by some amount, say Δx. This shifting results in a new "family" of fringes, which correspond to lines of constant $(\Delta N_x/\Delta x)$. Hence, if the shifted Δx is relatively small, such that the quantity $(\Delta N_x/\Delta x)$ approximates a true derivative, then these new fringes represent lines of constant strain, i.e., $e_x = \partial u_x/\partial x \approx (\Delta N_x/f\Delta x)$, where f = virtual reference grating frequency A similar approach can be used to obtain the other derivatives required to characterize the in-plane strain field, specifically $e_y = \partial v_y/\partial y$ and $e_{xy} = (1/2)(\partial u_x/\partial y + \partial v_y/\partial x)$.

Mechanical differentiation can be performed "directly" (i.e., using two transparencies as described in the preceding paragraph) or "indirectly". One indirect method is the use of double-exposure photography[17][24]. In this case a single sheet of photographic film is mounted within a moveable film holder, and is exposed twice to the same moiré fringe pattern. The film is shifted slightly between exposures. This approach is the optical equivalent to the physical shifting previously described, and results in a family of fringes representing constant strain. In a second indirect approach[25] a digitized image of the original moiré pattern is created and displayed on a CRT screen using appropriate computer-based hardware and software. A computer program then generates two versions of the digitized image, shifts one image with respect to the other, and displays both simultaneously. This procedure is the

numerical equivalent to the physical shifting of two transparencies, and again results in fringes of constant strain.

An experimental methodology similar to mechanical differentiation is the use of a reference grating whose frequency has been adjusted so as to cancel a uniform portion of the displacement field.[26]. In this case the remaining fringes are related to local non-uniformities in the overall displacement field.

Data Reduction by the Displacement-Field Approach

Another category of reducing moiré fringe patterns to strains includes methods based upon the "displacement-field approach"[24]. The technique is illustrated in Figure 5 and 6. A straight line which passes through a point of interest, such as line AB in Figure 5, is identified. The resulting displacements along this line are plotted. The slope of the displacement curve is the desired measure of strain, e.g. $e_x = \partial u_x/\partial x \approx (\Delta N_x/f\Delta x)$.

The data reduction scheme used in the present study is an automated version of the displacement-field approach illustrated in Figures 5 and 6. The technique was automated through the use of modern digitizing and computer equipment. The two primary pieces of equipment required were an AST Turboscan Digitizer and a Macintosh II computer with a 40 MB hard disk drive and a 40 MB tape backup. The moiré patterns were first photographed with a 35 mm camera, and 203 x 254 mm (8 x 10 in) photographic prints were prepared, as described in a preceding section. Since the actual

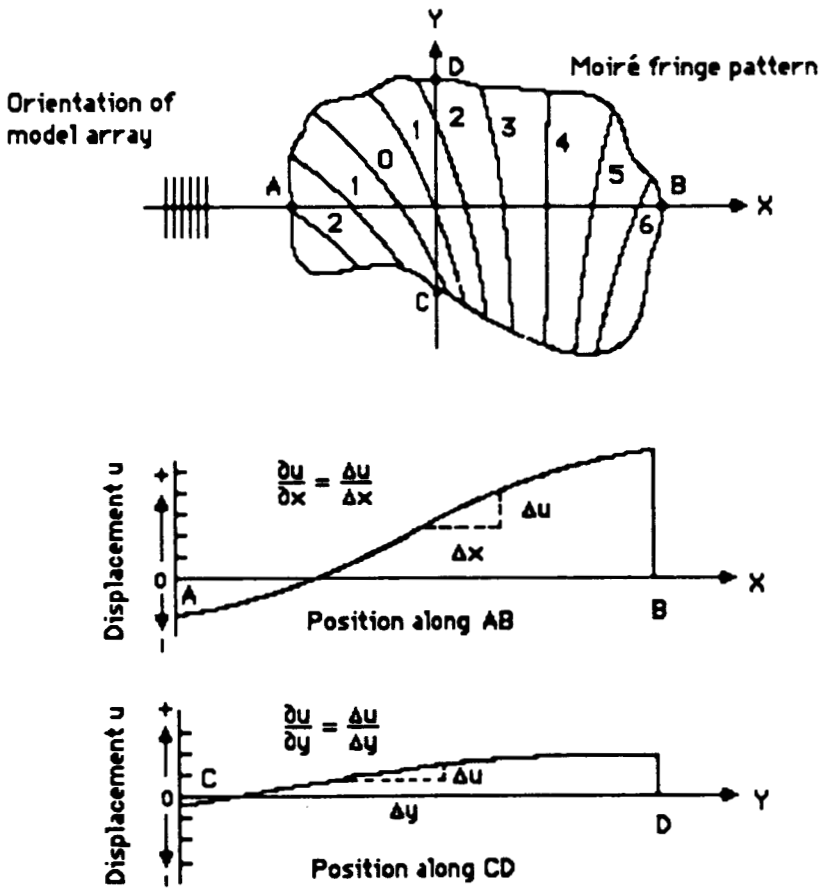

Figure 5: Displacement-Position Plots for ∂u/∂x and ∂u/∂y.[24]

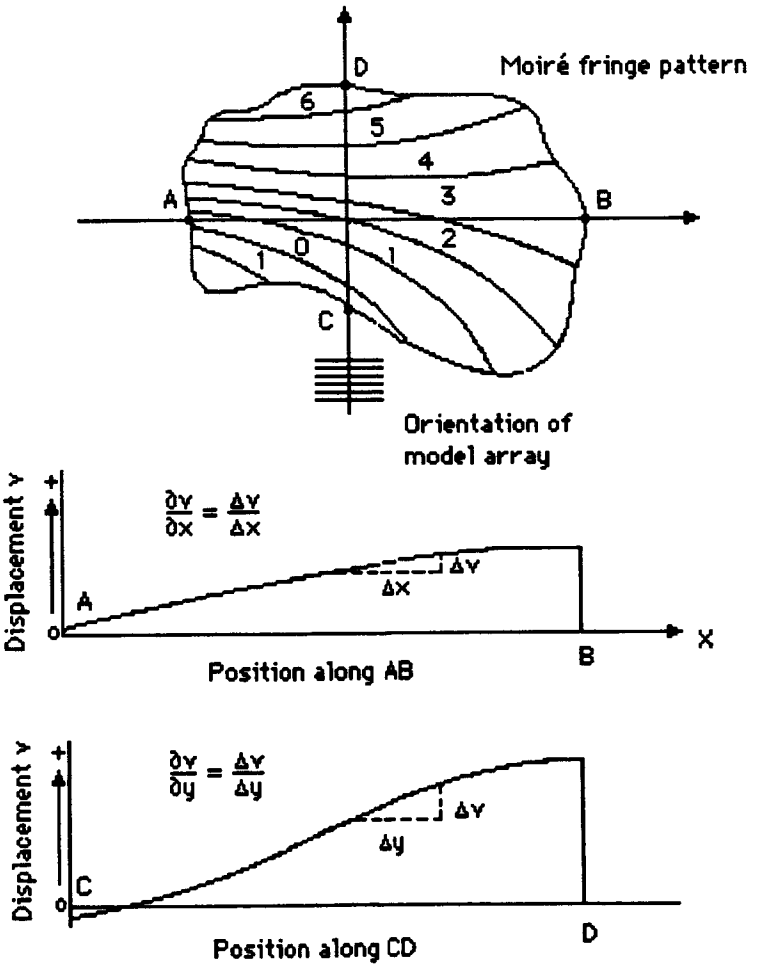

Figure 6: Displacement-Position Plots for ∂v/∂x and ∂v/∂y.[24]

grating size was 25 x 25 mm (1 x 1 in), the photographic prints represent a nominal optical magnification of 8X. A digital record of the moiré pattern is then obtained using the AST Turboscan Digitizer. This digitizer can be operated at a resolution ranging from 75 to 300 dots/in. In the present case the moiré photos were scanned at a resolution of 300 dots/in, resulting in an effective resolution of about 2400 dots/in. The AST Turboscan Digitizing software allows for editing of the scanned image. The software permits viewing and editing of the image at the pixel level. This allows the user to "clean up" any imperfections (such as dust particles, scratches, etc.) which appear in the image. Once the image is cleaned to an acceptable level the image is stored on disk or tape backup. An example of the above procedure is shown in Figures 7 and 8. Figure 7 shows the original photograph of a moiré pattern recorded for the y-displacements induced in an aluminum specimen with a hole, subjected to a 26 MPa (3770 PSI) compressive load. The specimen width and hole diameter are 25.4 mm and 6.35 mm (1 in and 0.25 in) respectively. Although this is a high-quality moiré image, note the various scratches and dust particles present. This image was scanned and "cleaned", resulting in the digital image shown in Figure 8.

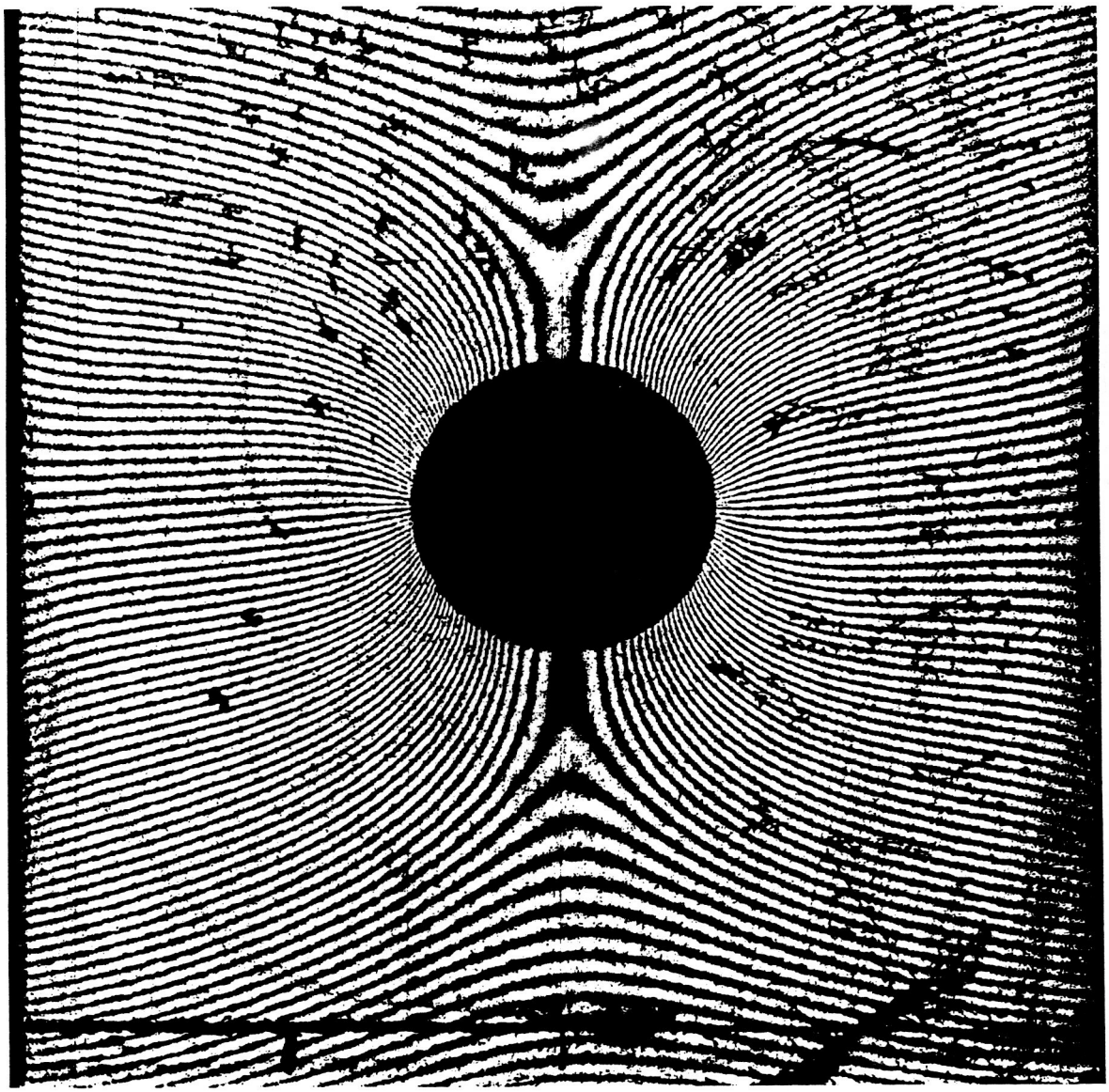

Figure 7: V-Displacement Field, Aluminum Specimen. (Original)

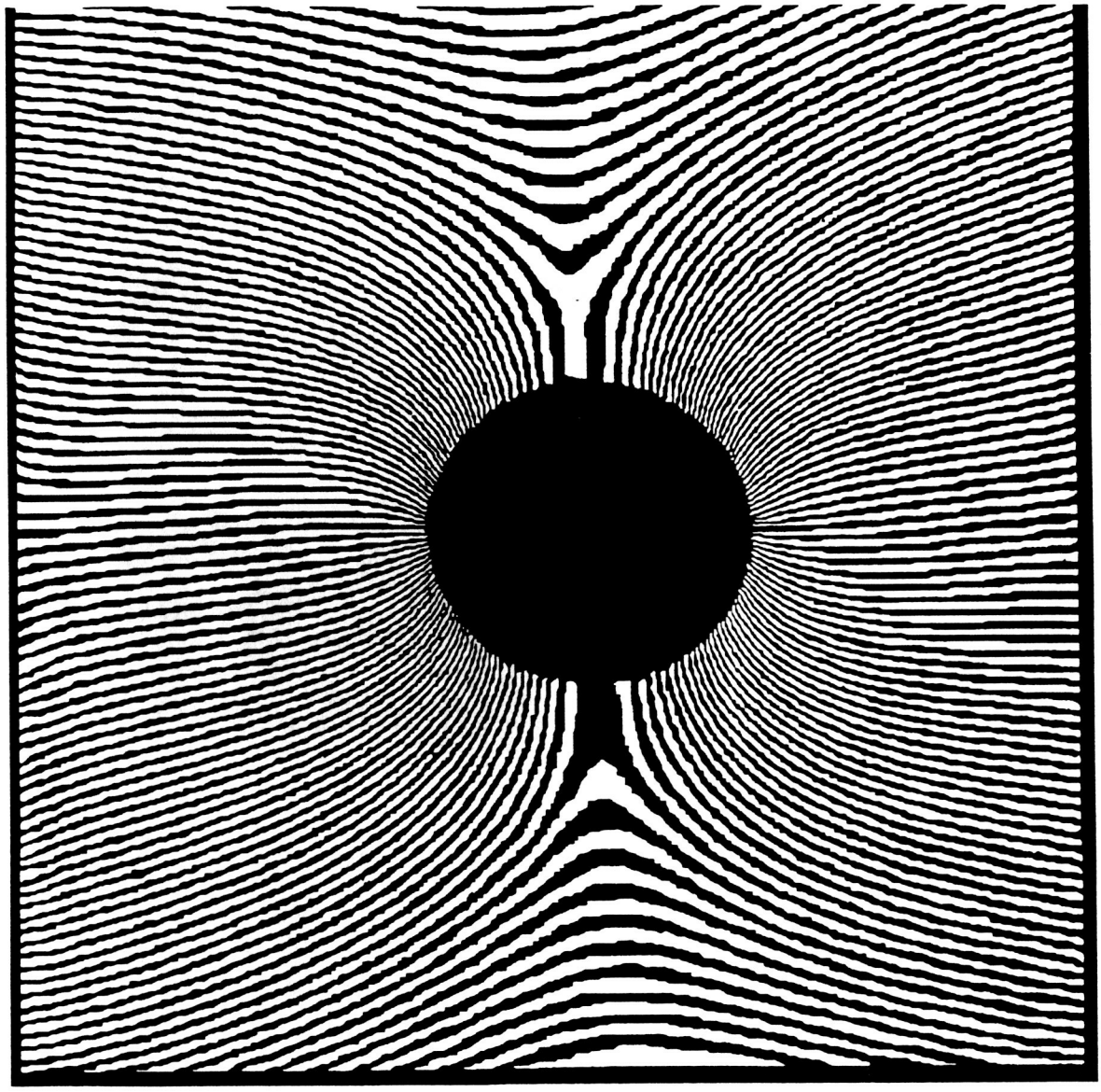

Figure 8: V-Displacement Field, Aluminum Specimen. (Clean)

After the digitization and cleaning process was complete the moiré data was reduced numerically using two computer programs developed in-house; programs "MOIRE" and "STRREG" (see Appendix A). Both programs were written using FORTRAN and standard Macintosh graphics software. Program MOIRE is used to convert the moiré fringe patterns to strains. Program STRREG is then used to create a strain contour plot which can be displayed on a computer monitor or plotted using a graphics printer. Details of each program are given in the following two sections.

Program MOIRE

The digitized moiré patterns created using the AST Turboscan system are stored in a bit map file, which in essence contains pixel information for every point on the image. The original 645 mm^2 (1 in^2) grating area is represented by 5,760,000 pixel points in the digitized image. The program MOIRE computes derivatives in either the horizontal or vertical directions. Normal strain e_x is determined from the u-displacement image, i.e. $e_x = du/dx$, while e_y is determined from the v-displacement image, i.e. $e_y = dv/dy$. Note that the shear strain e_{xy} can be found by taking the derivatives du/dy and dv/dx and summing them in the fashion: $e_{xy} = 1/2(du/dy + dv/dx)$. This latter calculation was not performed in this study.

Program MOIRE performs the above calculations in the following order:

1) The current scan line (in the case of strain e_x) or scan column, (in the case of strain e_y) is identified.

2) The data for the desired row or column is read from the image file. This data is stored as an 8 bit integer. The binary equivalent of this number represents a group of 8 pixels. A black pixel is stored with a 1 and a white pixel is stored with a 0. The 8 bit integer is converted to its binary equivalent and the pixel information is taken from each bit of this number and stored in a character array.

2) The center of each fringe is located by scanning the array and locating the edges of each fringe. The center of the fringe is assumed to be midway between each of the two fringe edges.

3) The appropriate derivative is calculated using the fringe center locations of three adjacent fringes (see Figure 9). For example, suppose the strain $e_x = du/dx$ is being calculated at fringe N_i, whose center is located at position x_i. The derivative is obtained using fringes immediately to the left and right of fringe N_i, i.e. fringes N_{i-1} and N_{i+1}, and so the derivative $e_x = du/dx$ can be approximated as:

$$\varepsilon_x = \frac{\Delta u}{\Delta x} = \left[\frac{(N_{i+1} - N_{i-1})}{f(x_{i+1} - x_{i-1})} \right]$$

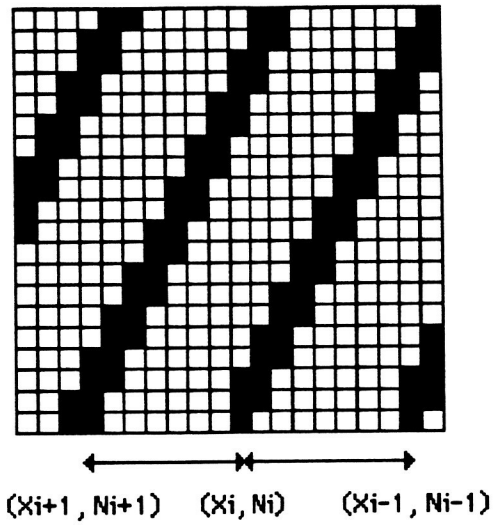

Figure 9: Fringe Center Locations

where:

f = virtual reference grating frequency

Noting that:

$N_{i+1} - N_{i-1} = \pm 2$

the above expression reduces to:

$$\varepsilon_x = \left[\frac{2^* scale}{f\left(x_{i+1} - x_{i-1}\right)}\right]$$

where:

scale = scale factor added to account for the difference in size of the original specimen and the computer image.

4) Strains are calculated at the center of each fringe along the entire row (or column), for every row (or column) in the image.

5) The strain values, along with the corresponding x and y coordinates, are stored in a file for use during stage two. The maximum and minimum values determined throughout the image are also recorded in a file.

Program MOIRE evaluates magnitudes of strain. The program does not use the actual fringe number when calculating strain, but rather relative fringe numbers that is, the fringe locations (N_{i-1} and N_{i+1}) used to calculate strains e_x or e_y, at fringe number N_i are assigned values of 1 and 3 respectively. This process thus calculates the absolute value of the strain for the given strain field.

The strain fields in this study were either compressive (in the case of axial strains) or largely tensile (in the case of transverse strains). In order to analyze complex strain fields which contain both compressive and tensile strains, a more rigorous determination of local fringe order is required.

Program STRREG

The strain field map is generated using program STRREG. The strain map is generated using the file containing x and y coordinates and either e_x or e_y, and from the file containing the maximum and minimum strain values.

1) The total range of strain, as determined using the maximum and minimum strain values, is broken up into eight intervals. A distinctive graphics pattern is assigned to each strain interval.
2) Each calculated strain value and corresponding x- and y-coordinates are read from the strain file.
3) STRREG opens a graphics window in memory, which is slightly larger than the original moiré displacement photograph. The x- and y-coordinates are found in the graphics window. The corresponding graphics pattern is assigned to that location, and plotted to the next coordinate location. If the local strain value has increased or decreased into a different strain interval, the graphics pattern is changed accordingly.
4) The strain field map is stored in a MacPaint™ format, allowing for easy editing and printing.

An example of the above approach is shown in Figure 10. The figure is based upon the original and digitized moiré fringe patterns previously presented in Figures 7 and 8, respectively.

Verification of the Data Reduction System

The data reduction system was verified by comparing the results obtained for an aluminum specimen to the elasticity solution for an infinite plate with a circular hole[24], and by comparison with a finite-element analysis for a finite-width plate. The elasticity solution is given by:

$$\sigma_r = \frac{\sigma_0}{2}\left\{\left(1-\frac{a^2}{r^2}\right)\left[1+\left(\frac{3a^2}{r^2}-1\right)\cos 2\theta\right]\right\}$$

$$\sigma_\theta = \frac{\sigma_0}{2}\left[\left(1+\frac{a^2}{r^2}\right)+\left(1+\frac{3a^4}{r^4}\right)\cos 2\theta\right]$$

$$\tau_{r\theta} = \frac{\sigma_0}{2}\left[\left(1+\frac{3a^2}{r^2}\right)\left(1-\frac{a^2}{r^2}\right)\sin 2\theta\right]$$

where

s_0 = remotely applied uniform stress

a = hole radius.

These equations were used to generate a data file containing x and y locations as well as axial strain values for an infinite plate with a hole. The STRREG program was then used to produce a strain field map. Figures 10 and 11 present the compressive axial strain fields determined for an aluminum plate using moiré interferometry, the elasticity solution for an infinite plate, and a finite-element solution for a finite width plate, respectively. The comparison between measurement and theory is considered to be reasonable. The discrepancies which do exist, in the case of the elasticity solution, are due to the fact that this solution is valid for an infinite plate, while the experimental measurements were obtained using a specimen of finite size. The finite-element results, which assumes a finite width plate, shows a much better correlation.

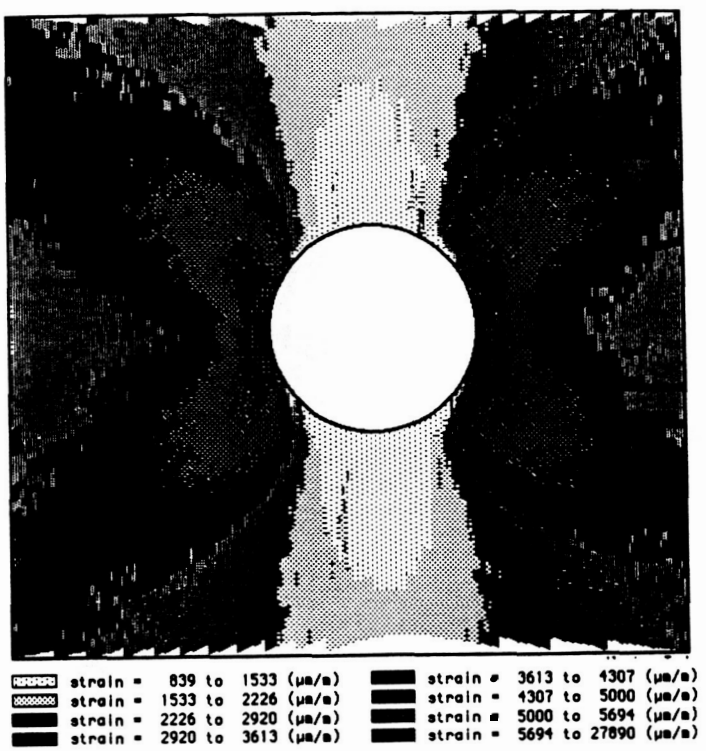

Figure 10: Axial Strain Field Map for an Aluminum Specimen
(Compressive Strains)

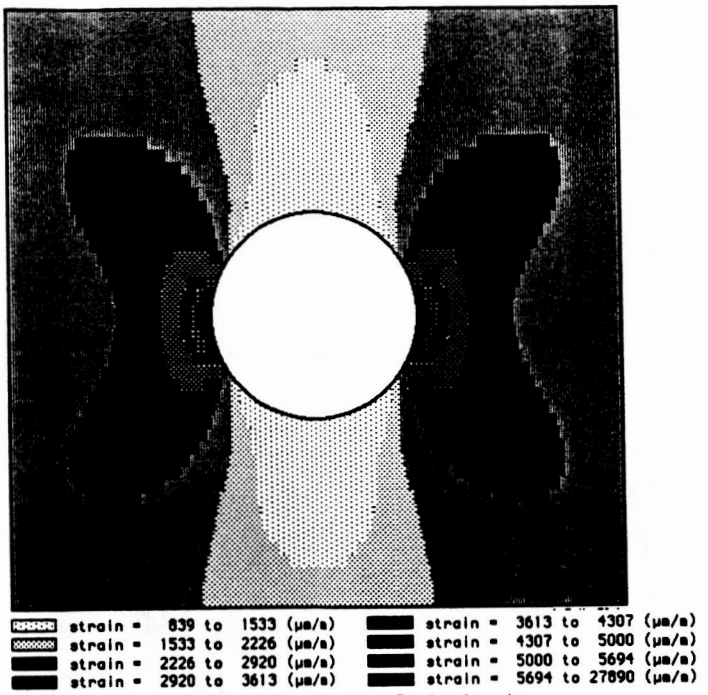

A: Infinite Plate (Elasticity Solution)

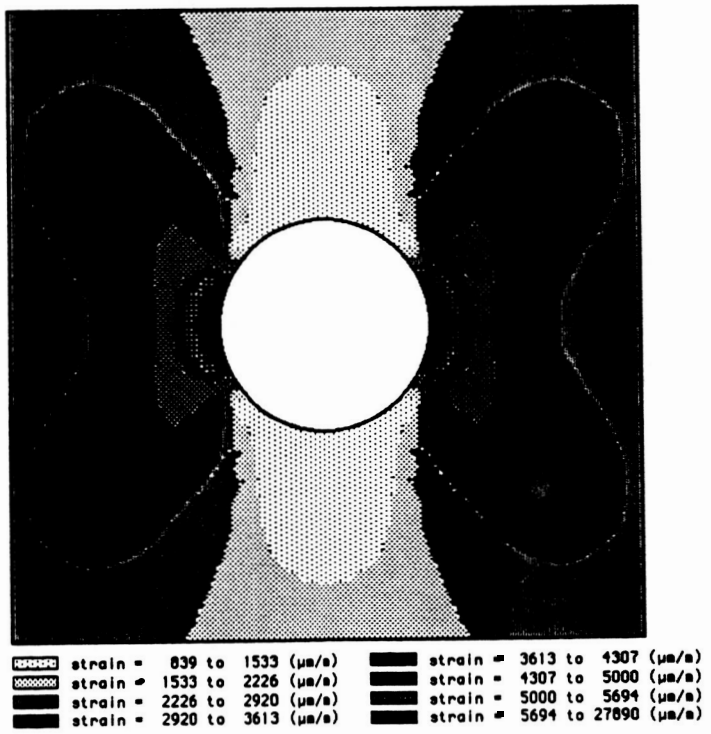

B: Finite-Element

Figure 11: Axial Strain Field Maps Theoretical Solutions
(Compressive Strains)

RESULTS

The results of the moiré analysis will be presented in two separate sections below. Each test will be briefly discussed in an individual subsection. The tests involving specimens without holes will be described first, followed by a description of the tests involving specimens with holes.

Specimens Without Holes

Specimen type A: $[0]_{48}$ Gr/Ep with no hole

This specimen was tested at a creep stress level of -496 MPa (-72,000 psi), corresponding to 78% of ultimate stress. The strains measured for this specimen were used to calculate E_{11} and n_{12}. Specifically, program MOIRE was used to calculate the axial and normal strains (e_1 and e_2, respectively) induced throughout the gage section of the specimen. The average strain measurements were then determined to be:

$$e_1 = -2982 \ \mu m/m$$

$$e_2 = 1632 \ \mu m/m$$

These measurements correspond to the following values for the "major" Young's modulus and Poisson's ratio:

$$E_{11} = 166.3 \text{ GPa}$$

$$n_{12} = 0.5473$$

These values compare well with similar results previously reported for Gr/Ep material systems[27]. Note the rather large value of n_{12}. This high value is typical of Gr/Ep material systems. For these

materials Poisson's ratio is considerably higher in compression than in tension. For example, in Reference [28] values of ν_{12} ranging from about 0.3 to 0.25 are reported for tensile loadings, while values ranging from about 0.55 to 0.63 are reported for compressive loadings.

Specimen type C: $[90]_{48}$ Gr/Ep with no hole

This specimen was initially tested at a creep stress level of -186 MPa (90% of the ultimate strength). This stress level resulted in a moiré pattern which was far too dense for analysis. A reduction in stress level was therefore required; the stress was first reduced to -83 MPa and subsequently to -33 MPa (40% and 16% of ultimate strength, respectively). When the stress was reduced to this latter value a moiré pattern with an acceptable fringe density was induced.

The strains measured for this specimen were used to calculate E_{22} and ν_{21}. The axial and normal strains (ε_2 and ε_1, respectively) induced throughout the gage section were determined using program MOIRE, and the average strain measurements were calculated as:

$$\varepsilon_2 = -4143 \quad \mu m/m$$

$$\varepsilon_1 = \quad 138 \quad \mu m/m$$

These measurements correspond to the following values for the "minor" Young's modulus and Poisson's ratio:

$$E_{22} = 7.97 \text{ GPa}$$

$$\nu_{21} = 0.0333$$

The measured value of E_{22} corresponds well with that reported in Ref [28].

The experimental measurements of E_{11}, E_{22}, n_{12} and n_{21} were evaluated to determine whether the following reciprocal relationship[1] was satisfied:

$$n_{21} = n_{12}(E_{22}/E_{11})$$

Using the measured for E_{11}, E_{22} and n_{12} listed above, the predicted value for the minor Poisson's ratio is n_{21} = 0.0262. Hence, the measured value of 0.033 deviated from the "expected" value by about 22%. This agreement is considered to be within the bounds of experimental error. The error represents the sum total of the errors in measuring each quantity, although it is likely due to a high percentage error in measuring n_{21}, due to the very small transverse strains involved in the direct measurement of this quantity.

The values of the measured moduli for the unidirectional graphite-epoxy specimens are summarized in Table 3.

Specimen Type B: $[0/45/0/-45]_{6s}$ Gr/Ep with no hole

The specimen was tested at a creep stress level of -399 MPa (-57,900 psi), corresponding to 63% of ultimate strength. The axial and transverse strains (e_y and e_x, respectively) were determined using program MOIRE. The average values were:

$$e_y = -4442 \ \mu m/m$$

$$e_x = 3769 \ \mu m/m$$

These measurements correspond to the following effective elastic moduli:

$$E_{yy} = 89.8 \text{ GPa}$$

$$n_{yx} = 0.8485$$

These measured values were compared with the predictions obtained using a commercially-available computer program based upon classical lamination theory[29]. In the CLT analysis the measured values for E_{11}, E_{22} and n_{12} described above were assumed. The shear modulus G_{12} was estimated as $G_{12} = 7.0$ GPa, based upon tabulated values in Ref [29]. The predicted effective moduli based upon the CLT analysis were:

$$E_{yy} = 83.5 \text{ GPa}$$

$$n_{yx} = 0.9545$$

Thus, the predicted and measured effective modulus and Poisson ratio differed by 7.5% and 11% respectively.

Specimen Type D: $[90/-45/90/45]_{6s}$ Gr/Ep with no hole

The specimen was tested at a creep stress level of -115 MPa (-16,700 psi), corresponding to 29% of ultimate strength. The axial and transverse strains (e_y and e_x, respectively) were determined using program MOIRE. The average values were:

$$e_y = -5382 \ \mu m/m$$

$$e_x = 906 \ \mu m/m$$

These measurements correspond to the following effective elastic moduli:

$$E_{yy} = 21.4 \text{ GPa}$$

n_{yx} = 0.1683

These measured values were compared with the predictions obtained using classical lamination theory. The predicted values were:

E_{yy} = 21.3 GPa

n_{yx} = 0.244

Thus, the predicted effective modulus and Poisson ratio differed by 0.5% and 31% from measured values, respectively. Note the rather large discrepancy between measured and predicted Poisson ratios in this case. The reason(s) for this discrepancy have not been identified.

The comparisons between measured and predicted moduli for the multi-angle laminates are summarized in Table 3.

TABLE 3

MEASURED AND PREDICTED MODULI FOR Gr/Ep LAMINATES

Modulus	Specimen type*	Measured Moduli	Predicted Moduli
E_{11}	Gr/Ep	166.3 GPa	NA
E_{22}	Gr/Ep	7.97 GPa	NA
n_{12}	Gr/Ep	0.5473	NA
n_{21}	Gr/Ep	0.0333	0.0262
E_{yy}	B	89.8 GPa	83.5 GPa
n_{yx}	B	0.8485	0.9545
E_{yy}	D	21.4 GPa	21.3 GPa
n_{yx}	D	0.1683	0.244

* Specimen types are defined as follows:

Gr/Ep IM7-8551 graphite-epoxy
Type B IM7-8551 graphite-epoxy $[0/45/0/-45]_{6s}$
Type D IM7-8551 graphite-epoxy $[90/-45/90/45]_{6s}$

Specimens With Holes

Specimen Type A: $[0]_{48}$ Gr/Ep with 6.35 mm dia hole

This specimen was tested at a creep stress level of -330 MPa (-47,900 psi), corresponding to 62% of ultimate strength. A "splitting" crack formed immediately upon application of the creep load. Although the crack was quite distinct and clearly visible, the

specimen supported the -330 MPa creep load, and hence was not considered to have "failed." The crack was very evident in the moiré patterns, as shown in Figures 12 and 13. These photographs were taken 1 minute after application of the load. As indicated, the crack initiated at the top and bottom edges of the holes, and extended approximately 6.35 mm (.25 in) into the gage section in both directions. The creep stress was held constant throughout the 10 hr test. No apparent crack extension occurred during the test; the moiré patterns recorded after 10 hrs were essentially identical to those shown in Figures 12 and 13.

The axial strain distributions calculated at a creep time of 1 min and 10 hrs are presented in Figures 14 and 15 respectively. The crack had no effect on axial strain distribution, and is not at all apparent in these figures. No significant strain redistribution occurred during the 10 hr creep test. Axial strains were a maximum at the "3-o'clock" and "9-o'clock" positions around the hole, as would be expected. The overall distribution of axial strains is highly elongated in the fiber/loading direction. It is interesting to compare this axial strain distribution with the axial strain distribution for an isotropic aluminum plate, as presented in Figure 10.

Equivalent results for the transverse strains are presented in Figures 16 and 17. In this case the existence of the crack is clearly evident in regions near the crack tip. Since the transverse strains were tensile, the crack tips were subjected to Mode I loading.

Observe that the transverse strain plots include a small "island" of high strain in the immediate vicinity of the crack tip. These islands are reminiscent of the isochromatic fringe "loops" normally seen for Mode I loading of a crack when using photoelastic techniques[30]. No significant transverse strain redistribution occurred during the 10 hr creep test. The u-displacement field (Figure 13) shows two regions (on the left and right sides of the hole) where the transverse strain changes sign, i.e., become compressive. As previously mentioned program MOIRE does not assign an algebraic sign to computed strains. The transverse strain field, therefore, does not indicate the small regions of compressive strain in the predominantly tensile strain field.

A finite-element analysis was performed for this specimen geometry. The material properties used during the analysis have been previously listed in Table 3. The axial and transverse strain distributions predicted using the finite element analysis are presented in Figures 18 and 19, and should be compared with the experimental results in Figures 14 and 16 respectively. The comparison between measured and predicted axial strain distributions (Figures 14 and 18 respectively) is very good. Some differences in strain magnitudes are apparent, in particular near the regions of highest axial strains (the "3-o'clock" and "9-o'clock" positions). Nevertheless, the overall strain distributions agree very well.

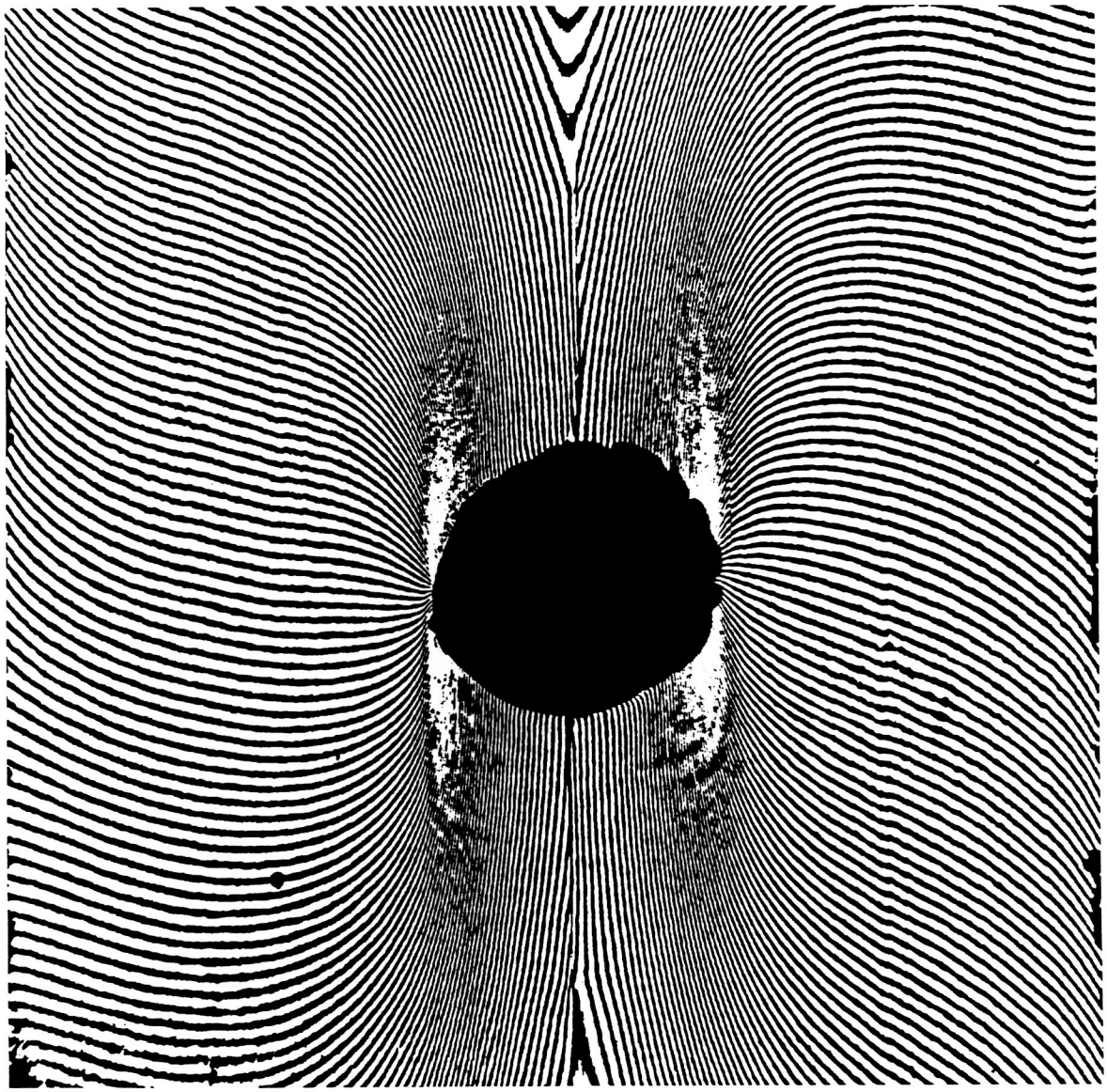

Figure 12: V-displacement Field, $[0]_{48}$, t = 1 min.

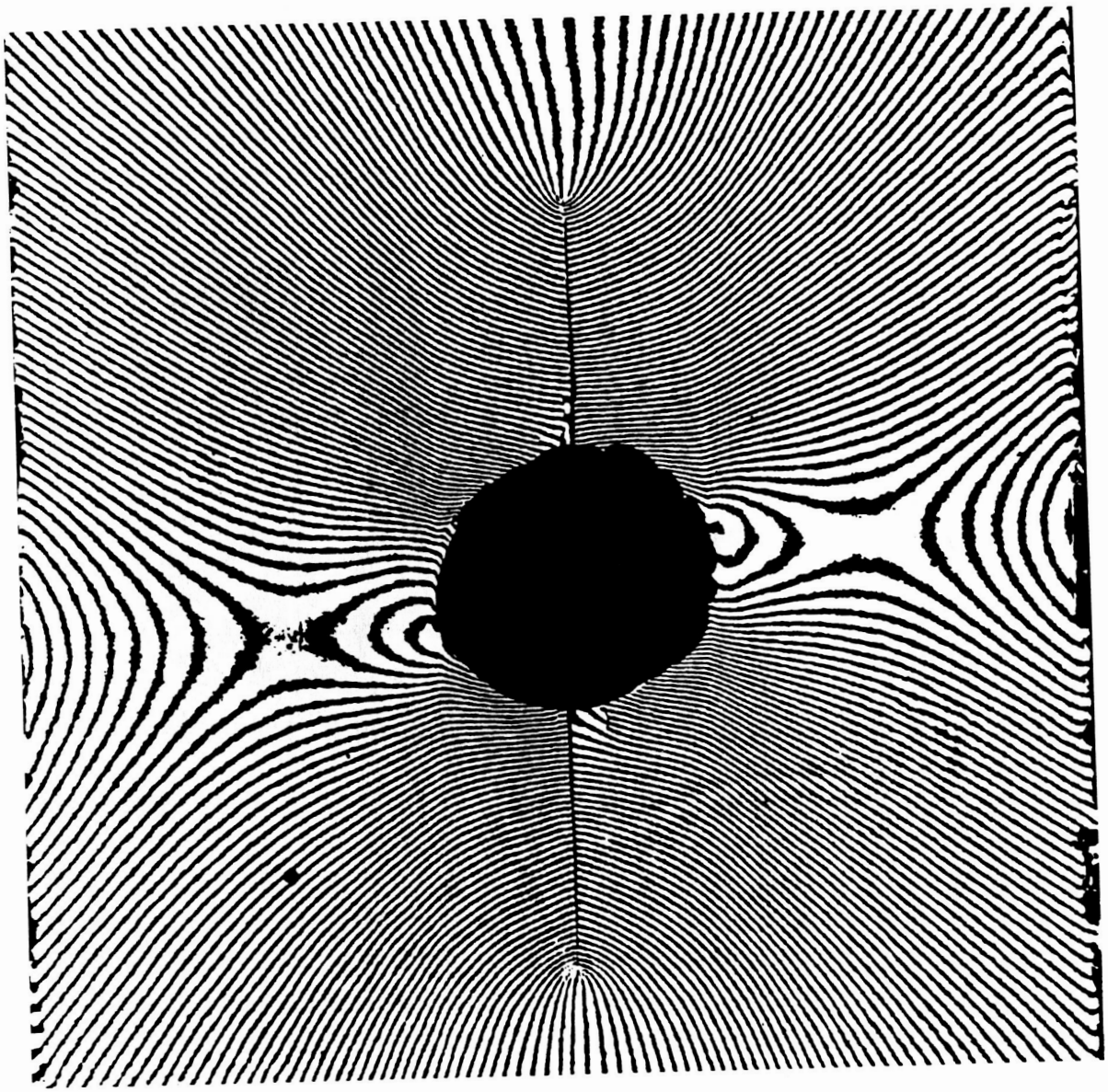

Figure 13: U-Displacement Field, $[0]_{48}$, t = 1 min.

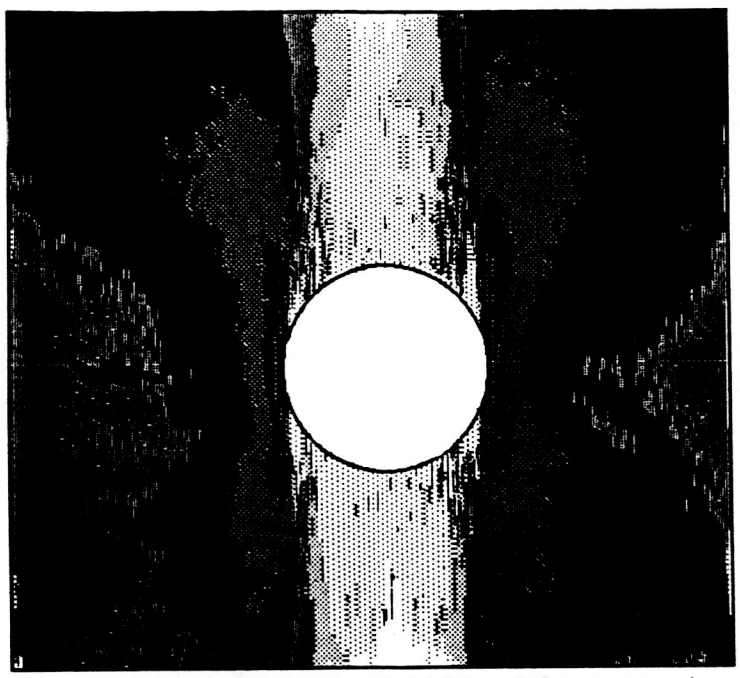

Figure 14: Axial Strain Field Map $[0]_{48}$, t = 1 min
(Compressive Strains)

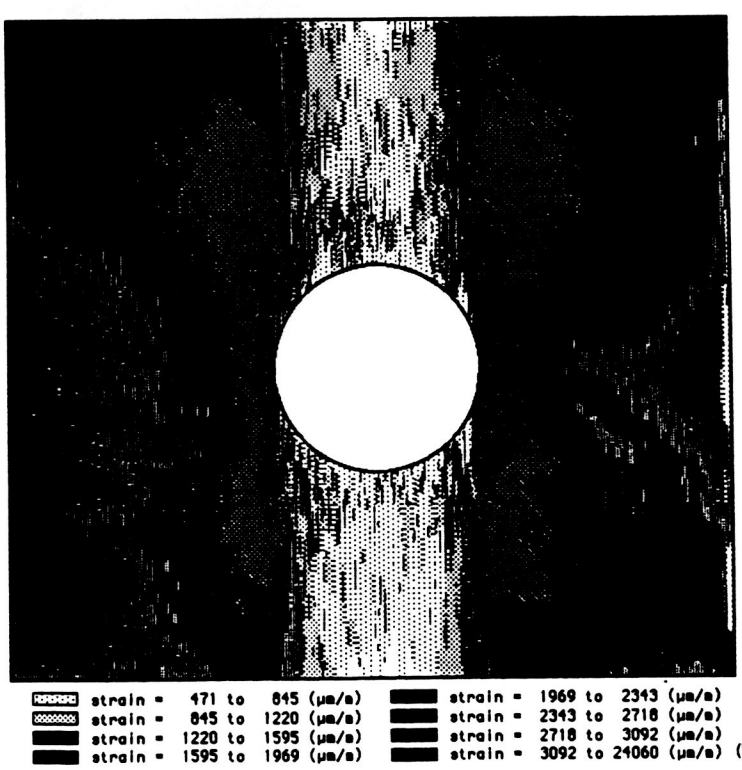

Figure 15: Axial Strain Field Map $[0]_{48}$, t = 10 hrs
(Compressive Strains)

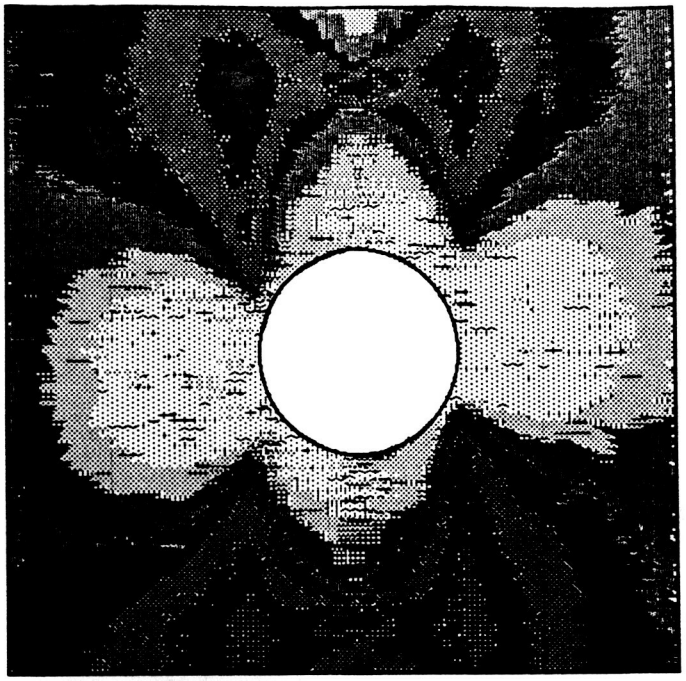

Figure 16: Transverse Strain Field Map $[0]_{48}$, t = 1 min
(Tensile Strains)

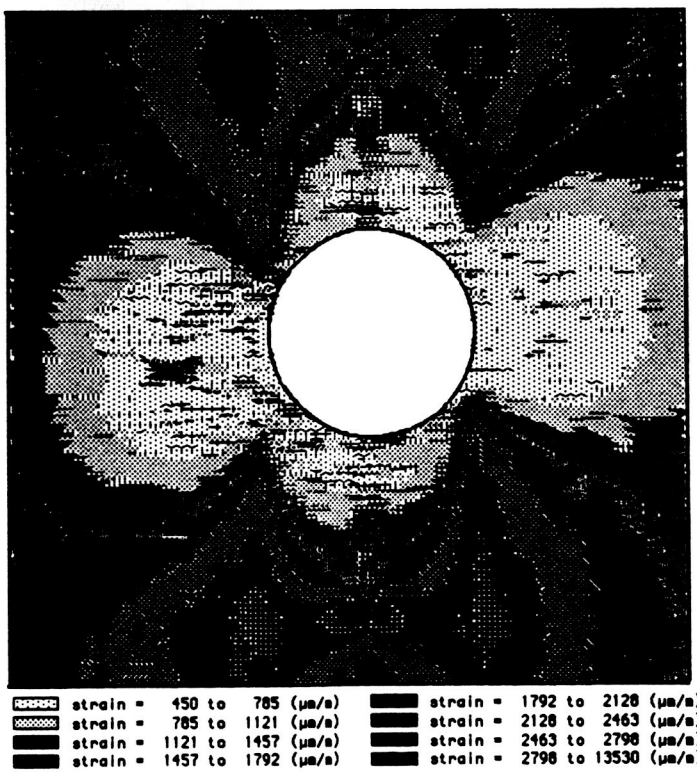

Figure 17: Transverse Strain Field Map $[0]_{48}$, t = 10 hrs
(Tensile Strains)

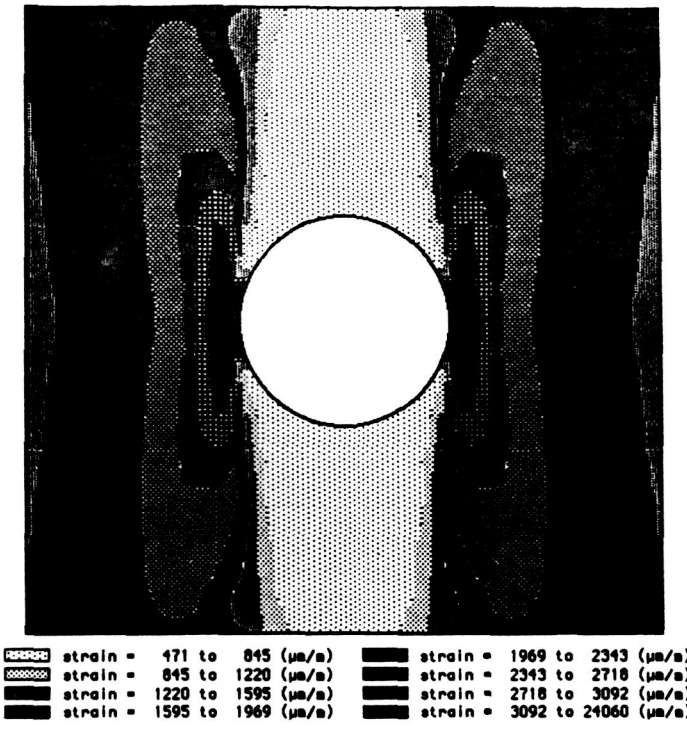

Figure 18: F.E. Axial Strain Field Map $[0]_{48}$
(Compressive Strains +)

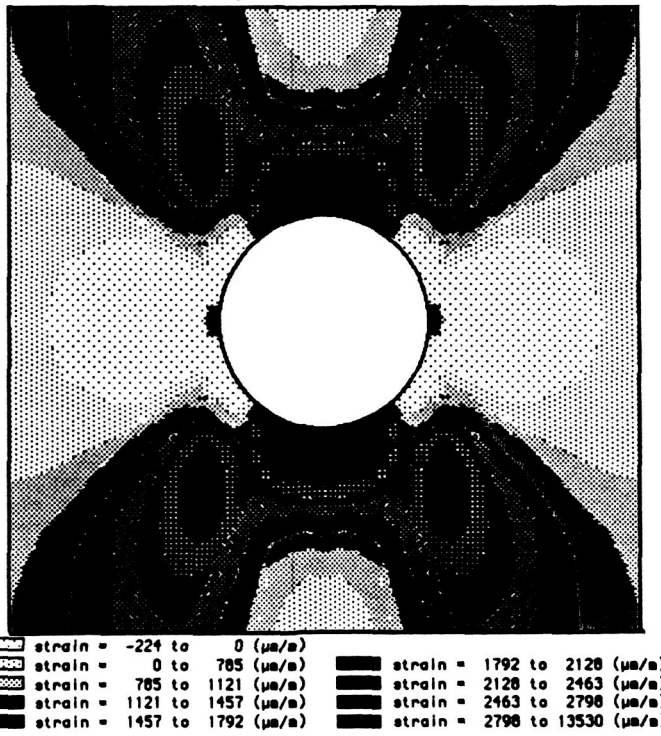

Figure 19: F.E. Transverse Strain Field Map $[0]_{48}$
(Tensile Strains +)

On the other hand, the comparison between measured and predicted transverse strains (Figures 16 and 19, respectively) is not so good. The difference is due to the existence of the crack. The predicted distribution shows a region of high transverse strain in the "12-o'clock" and "6-o'clock" positions. This is precisely where the splitting crack originated during the test. The existence of the crack unloaded material in the immediate vicinity of the hole, reducing transverse strains near the hole. Strains were redistributed such that a general increase in transverse strain at regions removed from the hole occurred. The finite element analysis predicts several regions of compressive strain, on the right and left sides of the hole, and also at the edge of the hole on ±45° diagonals. The experimental u-displacement field shows the two regions on the left and right sides of the hole, but the regions on the ±45° diagonals are not apparent.

Specimen Type C: $[90]_{48}$ Gr/Ep with 6.35 mm dia hole

This specimen was tested at a creep stress level of -66 MPa (33% of the ultimate strength). During the test severe grating degradation took place, resulting in excessive "noise" in the 10 hour strain field maps. The degradation resulted in an overall loss of reflection and refraction of the grating; the specimen grating appears to "cloud over". It is suspected that the degradation is due to oxidation of the grating. The phenomena occurs randomly, and was also occasionally encountered by Klein[12]. In the present test

the overall shape of the strain distributions was still evident, despite the degraded moiré pattern.

The axial strain distributions calculated at a creep time of 1 min and 10 hrs are presented in Figures 20 and 21 respectively. An analysis of the two figures shows that some strain redistribution occurred during the 10 hr creep test. This redistribution is most clearly evident in regions near the "12-o'clock" and "6-o'clock" positions. At time t = 1 min relatively large regions of small axial strain are evident at these locations, while at t = 10 hrs these regions have been significantly reduced in size. Upon further inspection the broad "winged" shaped regions, roughly defined by the ±45° directions, are seen to have generally expanded during the 10-hr creep test, indicating axial strain redistribution due to viscoelastic effects. Maximum axial strains occur at the sides of the hole, as in the type A specimen.

The transverse strain fields for the 1 min and 10 hr creep times are presented in Figures 22 and 23. The transverse strain fields also show strain redistribution during the 10 hr creep test. Notice that "loops" of high strain exist at the "3-, 6-, 9- and 12-o'clock" position around the hole. In the 10 hr strain field, these loops of higher strain have been expanded, indicating viscoelastic behavior.

The axial and transverse strain distributions predicted using the finite-element analysis are presented in Figures 24 and 25, and should be compared with the experimental results in Figures 20 and

22, respectively. The overall comparison between predicted and measured axial strains is considered to be reasonable, although differences in strain magnitudes are apparent. The finite-element prediction for the transverse strain field however, is very different from the strain field measured experimentally. The primary characteristic of the finite-element prediction is the highly elongated "lobes" of transverse strain, centered symmetrically above and below the hole. Also note that the predicted transverse strains are roughly one order of magnitude less than the measured transverse strains. In addition, the finite-element transverse strain field shows small regions of compressive strain at the edge of the hole on ±45° diagonals, as observed for the $[0]_{48}$ specimen. These small regions of compressive strain were not apparent in the experimentally-determined transverse strain field.

The discrepancies between prediction and measurement evidenced in this case is far greater than the discrepancies associated with any of the other comparisons considered during this study. The reason(s) for this isolated, but severe, discrepancy have not been identified. Perhaps the test specimen developed some significant internal defect upon application of the creep load, such as a large internal delamination, for example. Such a hypothesized defect was not apparent, however, and it is likely that if such a defect existed it would have been readily evident in the moiré pattern.

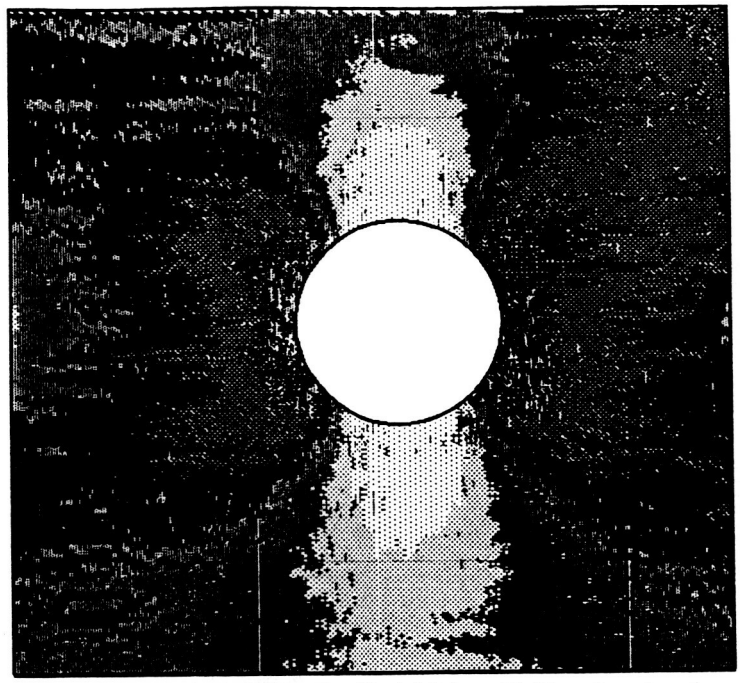

Figure 20: Axial Strain Field Map $[90]_{48}$, t = 1 min
(Compressive Strains)

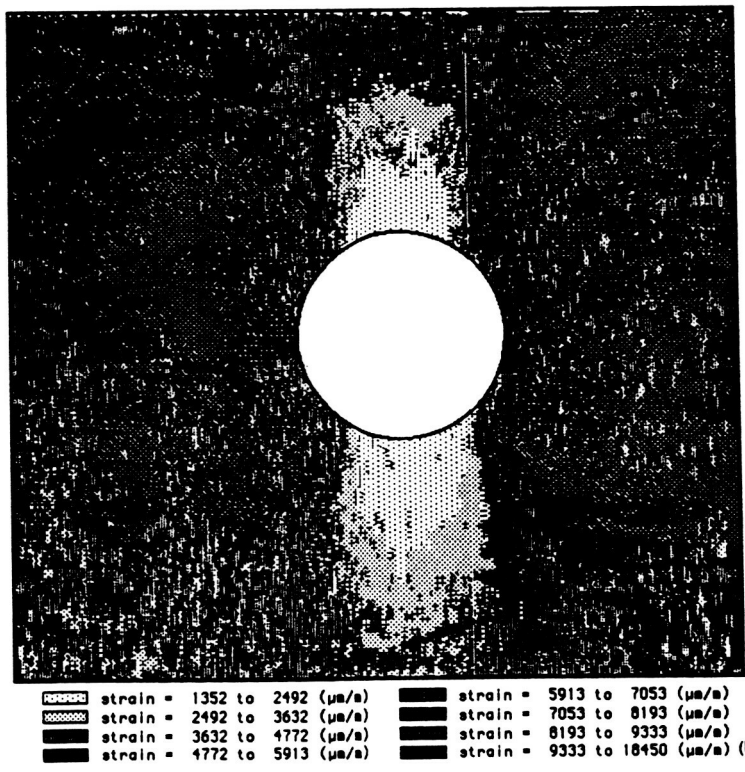

Figure 21: Axial Strain Field Map $[90]_{48}$, t = 10 hrs
(Compressive Strains)

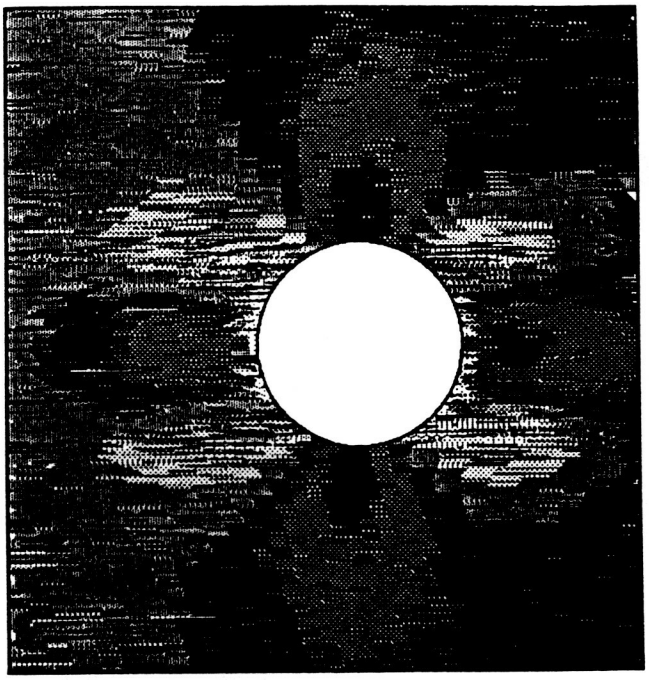

Figure 22: Transverse Strain Field Map $[90]_{48}$, t = 1 min
(Tensile Strains)

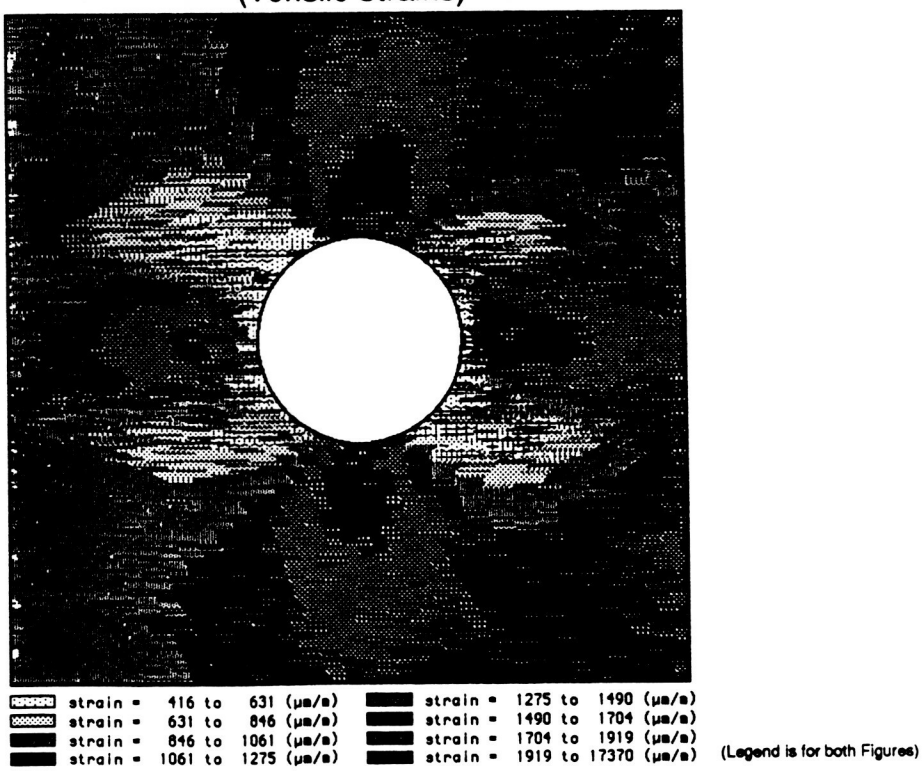

Figure 23: Transverse Strain Field Map $[90]_{48}$, t = 10 hrs
(Tensile Strains)

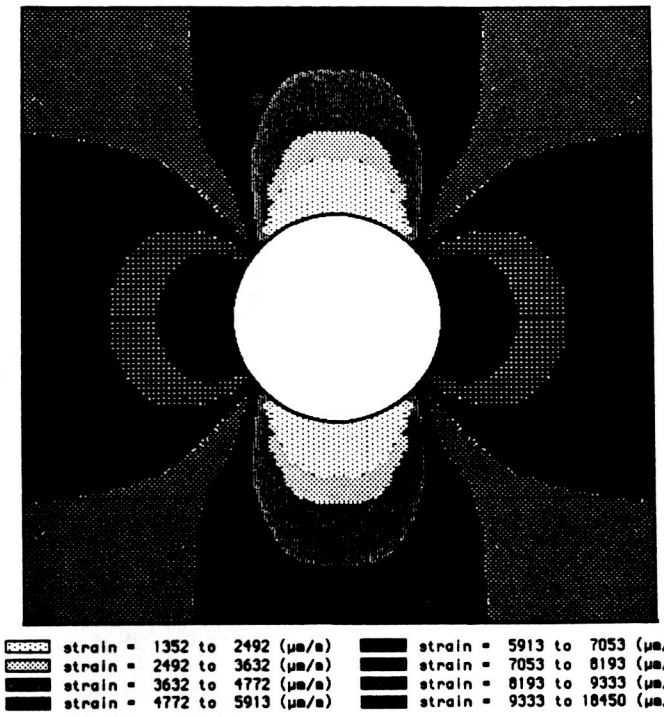

Figure 24: F.E. Axial Strain Field Map $[90]_{48}$
(Compressive Strains +)

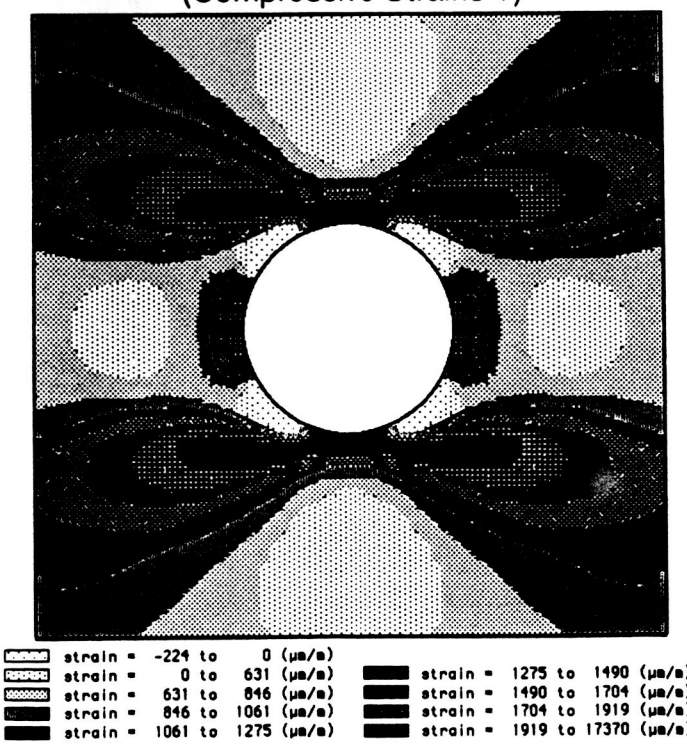

Figure 25: F.E. Transverse Strain Field Map $[90]_{48}$
(Tensile Strains +)

Specimen Type B: $[0/45/0/-45]_{6s}$ Gr/Ep with 6.35 mm dia hole

This specimen was tested at a creep stress level of -419 MPa (-60,770 psi), corresponding to 78% of ultimate strength. The moiré patterns associated with the v- and u-displacements obtained at t = 1 min are shown in Figures 26 and 27. Nearly identical u- and v-displacement fields for quasi-isotropic specimens with holes under tensile loading were reported by Post[2].

The axial strain field maps, shown in Figures 28 and 29, show no significant redistribution of strain during the 10 hr creep test. It is interesting to note that the disturbances in the strain field resulting from the hole, in the axial strain field do not extend as far from the hole as in the $[0]_{48}$ (type A) axial strain fields (Figures 14 and 15). The type B axial strain fields are similar in shape to those of the isotropic aluminum plate, shown in Figure 10.

The transverse strain fields for this specimen are presented in Figures 30 and 31. These strain fields also show no signs of viscoelastic behavior for the 10 hr creep test. Note that areas of high strain exist at the top and bottom of the hole as well as along ±45° diagonals extending away from the hole. Klein found similar double strain "peaks" in his analysis [Ref 12, Figure 28].

Finite-element strain field predictions are presented in Figures 32 and 33. A comparison of these results with the experimental results shows a very good overall correlation in both the axial and transverse strain distributions. However, the

finite-element transverse strain field shows small regions of compressive strain, not observed in the experimental strain field, at the edge of the hole on ±45° diagonals, just as in the $[0]_{48}$ specimen.

Specimen Type D: $[90/-45/90/45]_{6s}$ Gr/Ep with 6.35 mm dia hole

The specimen was initially tested at a creep stress level of -308 MPa (-44,671 psi), corresponding to 90% of the ultimate strength. This stress level resulted in an immediate delamination of the specimen on both sides of the hole. This delamination slowly grew with time. Figures 34 and 35 show the delamination growth for the specimen. Strain field maps were not generated for this specimen due to the extremely high fringe densities resulting from the delamination. Complete, catastrophic failure of the specimen occurred at about 16 hours after loading. The failed specimen is shown in Figures 36 and 37. The failed region of this specimen resembles the brooming failure observed for the ultimate strength test specimens. Note the relatively symmetric failure mode, indicating an absence of overall buckling failure. The growth of the delamination throughout the 16 hr test indicates viscoelastic behavior for this layup at room temperature, and also clearly shows the intimate relationship between viscoelastic and fracture mechanisms. Similar failures of a composite specimen subjected to fatigue loadings have been reported by Carlsson[32].

A second type D specimen was prepared and this specimen was tested at a creep stress level of -154 MPa (-22,335 psi), 45% of

the ultimate strength. The purpose of the second test was to see if viscoelastic effects would be evident at this lower stress level.

Figures 38 and 39 present the axial strain fields. There are signs of slight strain redistribution for this test; the level of redistribution is on the same order as that presented in Figures 20 through 23 for the type C $[90]_{48}$ specimen. It is important to note that viscoelastic behavior took place at room temperature over a 10 hr test period, at a stress level that was less than half of the ultimate stress. The shape of the strain fields are similar to those presented in the type B specimen layup.

Slight viscoelastic response can also be seen when comparing the 1 min and 10 hr transverse strain fields, presented in Figures 40 and 41. The transverse strain field shows the same general shape as the type B specimen with similar areas of strain concentrations. The transverse strain fields show areas of "jagged" edges, this results from the relatively few fringes in the u-displacement field and hence few data points. Comparisons of the finite-element strain field predictions, shown in Figures 42 and 43, to the experimental strain fields show very similar strain distributions in both the axial and transverse cases. However, the finite-element predicts small regions of compressive strain,at the edge of the hole on ±45° diagonals, just as in the other specimens. These areas of compressive strain were not apparent in the moiré patterns.

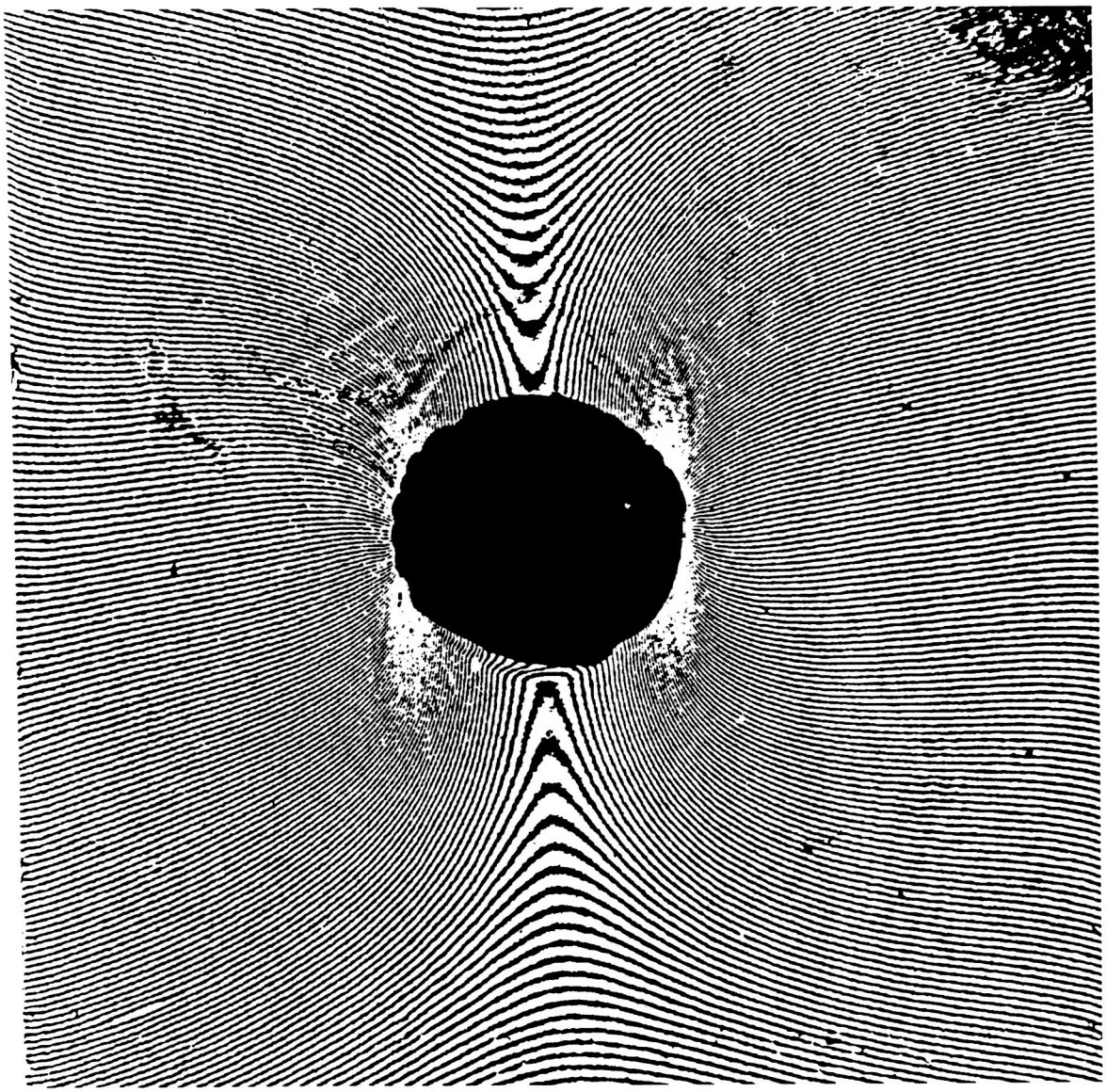

Figure 26: V-Displacement Field, $[0/45/0/-45]_{6s}$, t = 1 min.

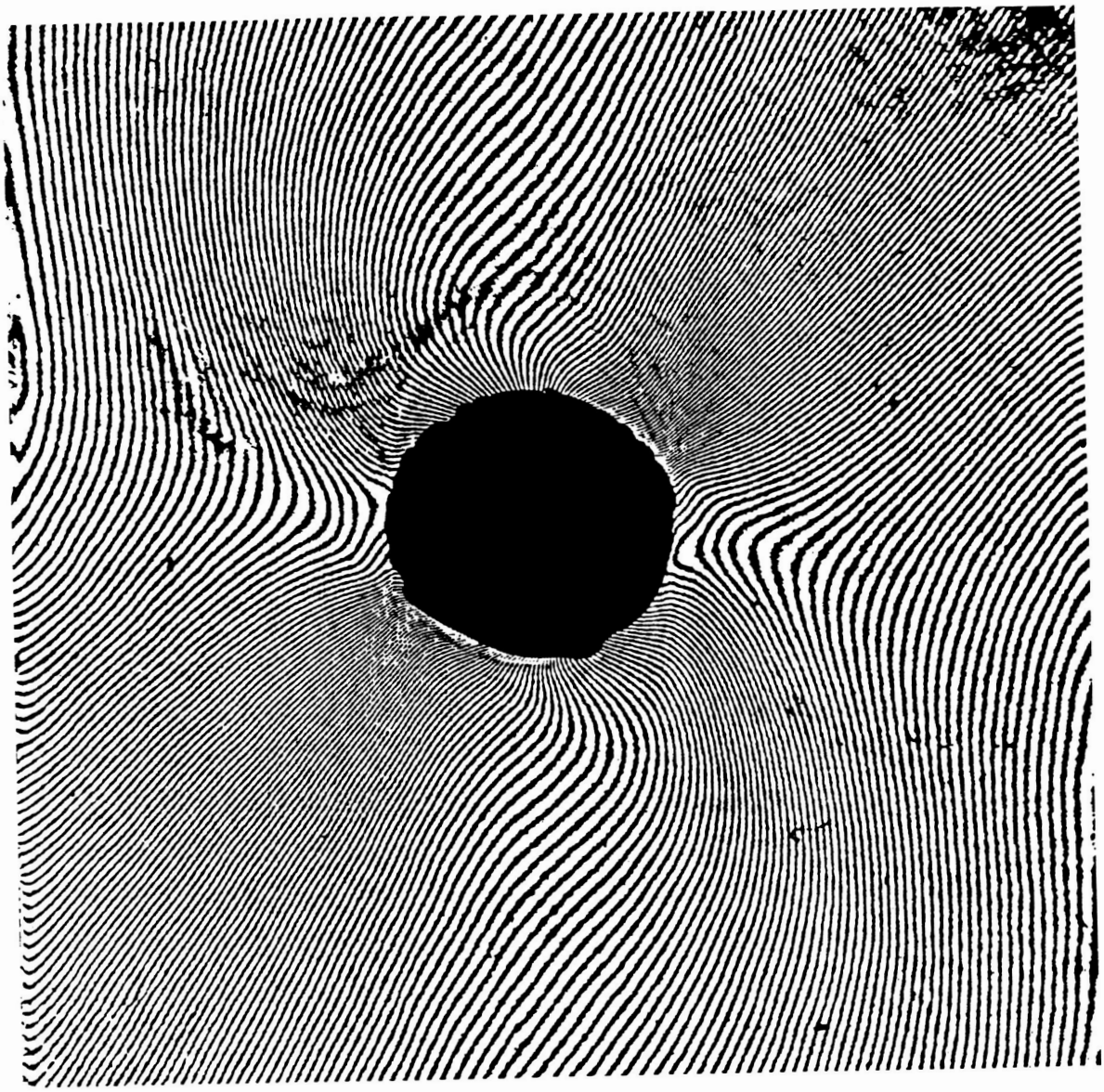

Figure 27: U-Displacement Field, $[0/45/0/-45]_{6s}$, t = 1 min.

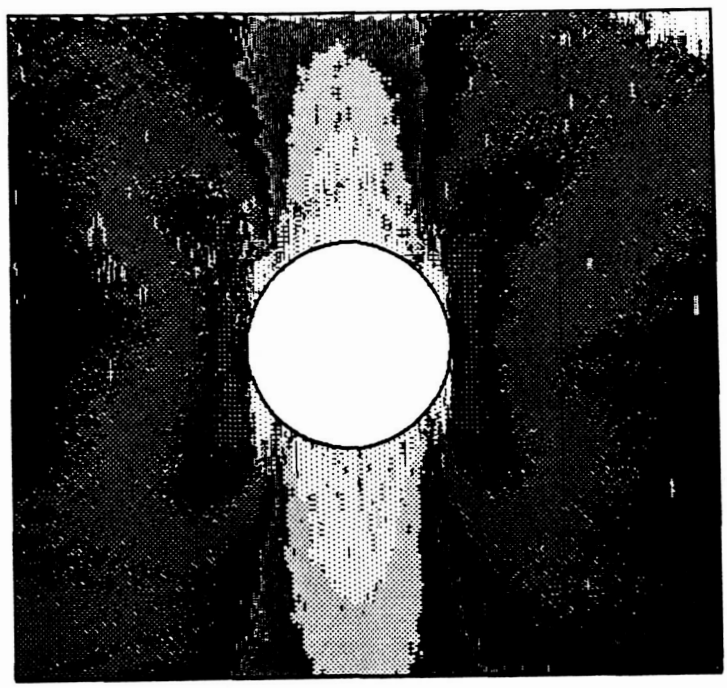

Figure 28: Axial Strain Field Map $[0/45/0/-45]_{6s}$, t = 1 min
(Compressive Strains)

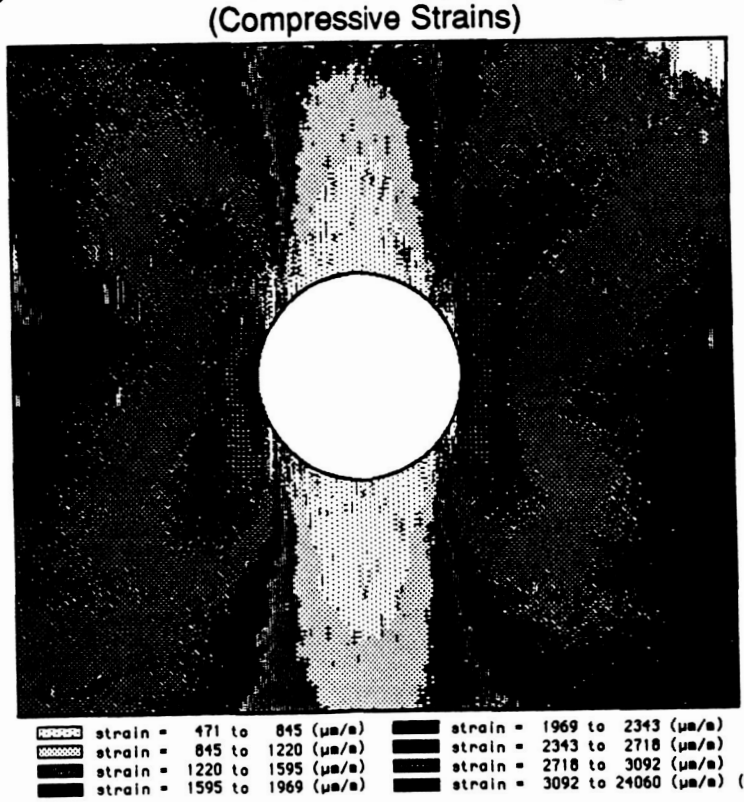

Figure 29: Axial Strain Field Map $[0/45/0/-45]_{6s}$, t = 10 hrs
(Compressive Strains)

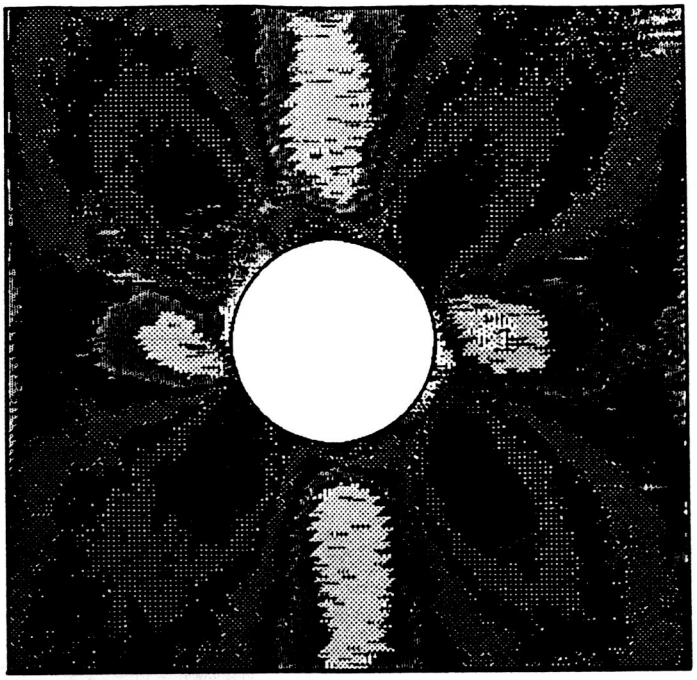

Figure 30: Transverse Strain Field Map $[0/45/0/-45]_{6s}$, t = 1 min
(Tensile Strains)

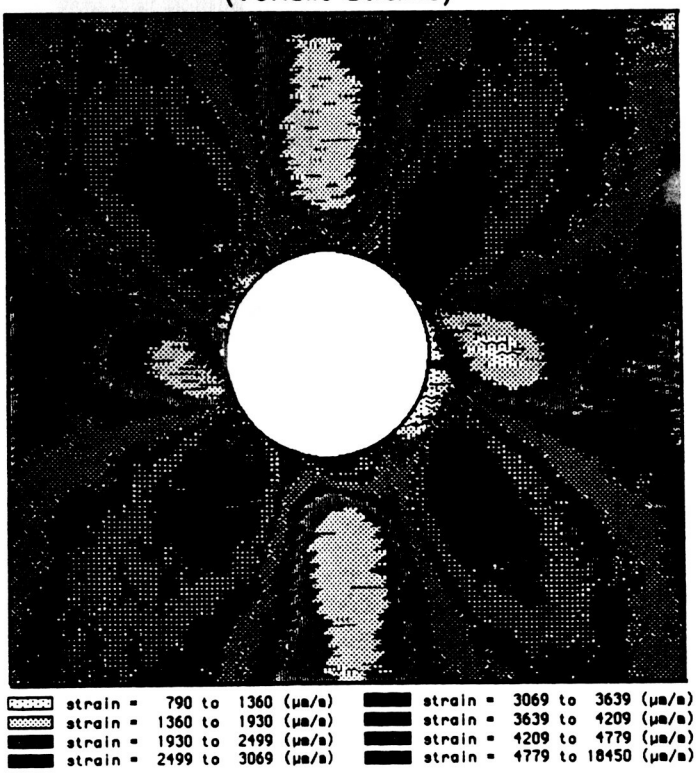

Figure 31: Transverse Strain Field Map $[0/45/0/-45]_{6s}$, t = 10 hrs
(Tensile Strains)

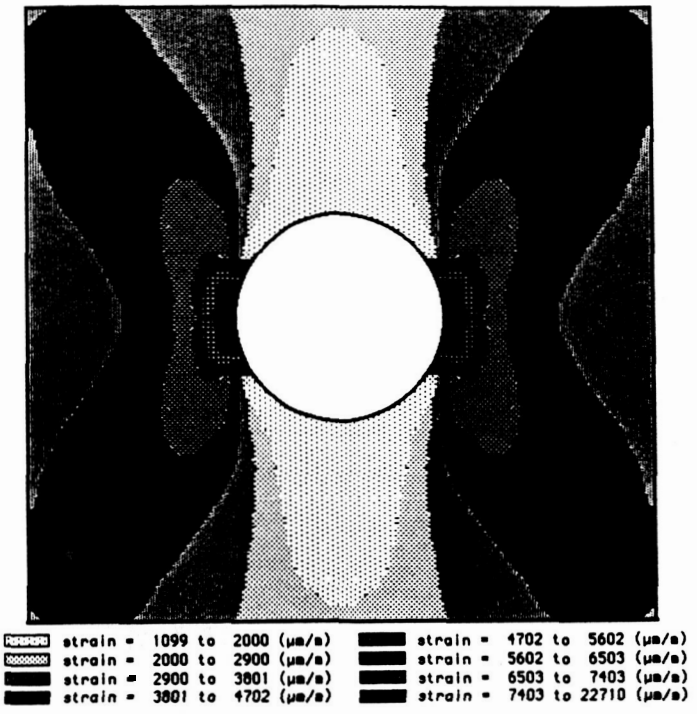

Figure 32: F.E. Axial Strain Field Map $[0/45/0/-45]_{6s}$
(Compressive Strains +)

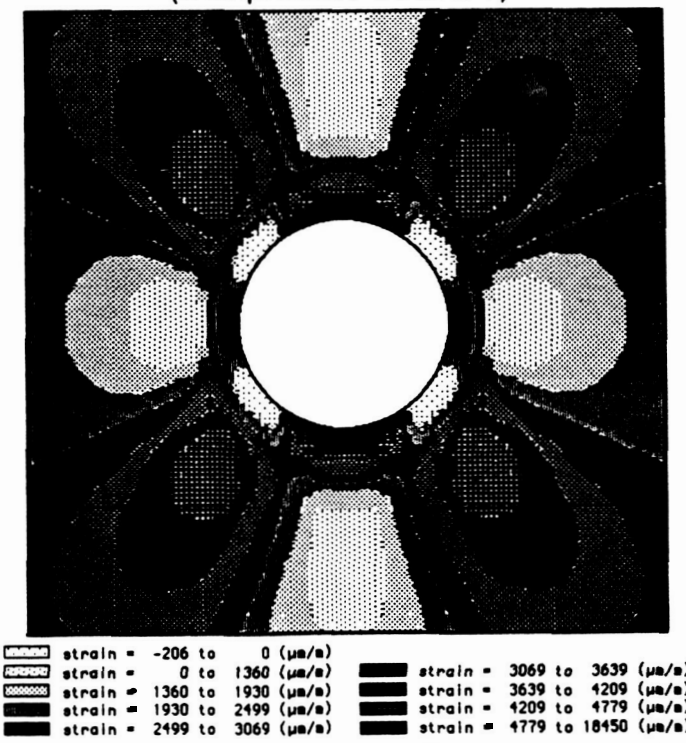

Figure 33: F.E. Transverse Strain Field Map $[0/45/0/-45]_{6s}$
(Tensile Strains +)

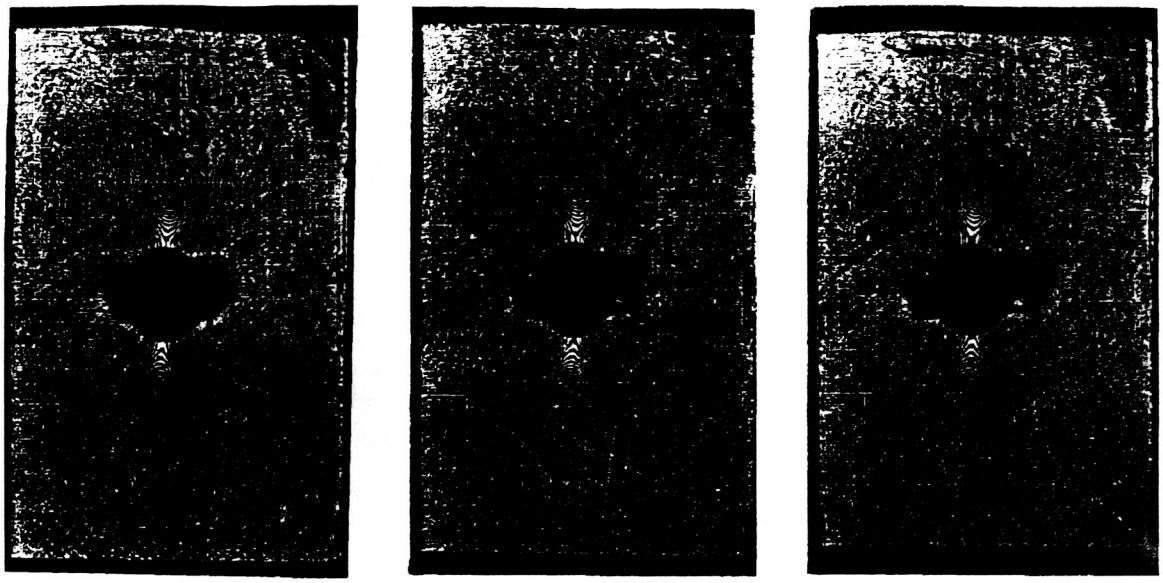

TIME = 1 MIN TIME = 10 MIN TIME = 30 MIN

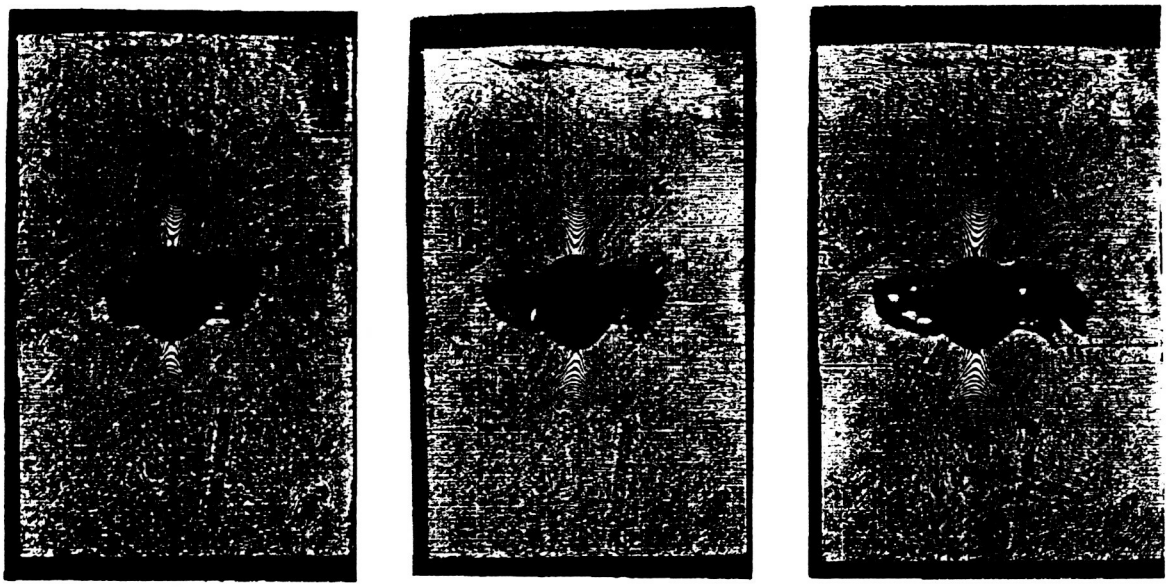

TIME = 1 HRS TIME = 5 HRS TIME = 10 HRS

Figure 34: Delamination of Type D $[90/45/90/-45]_{6s}$ Gr/Ep V-Displacement

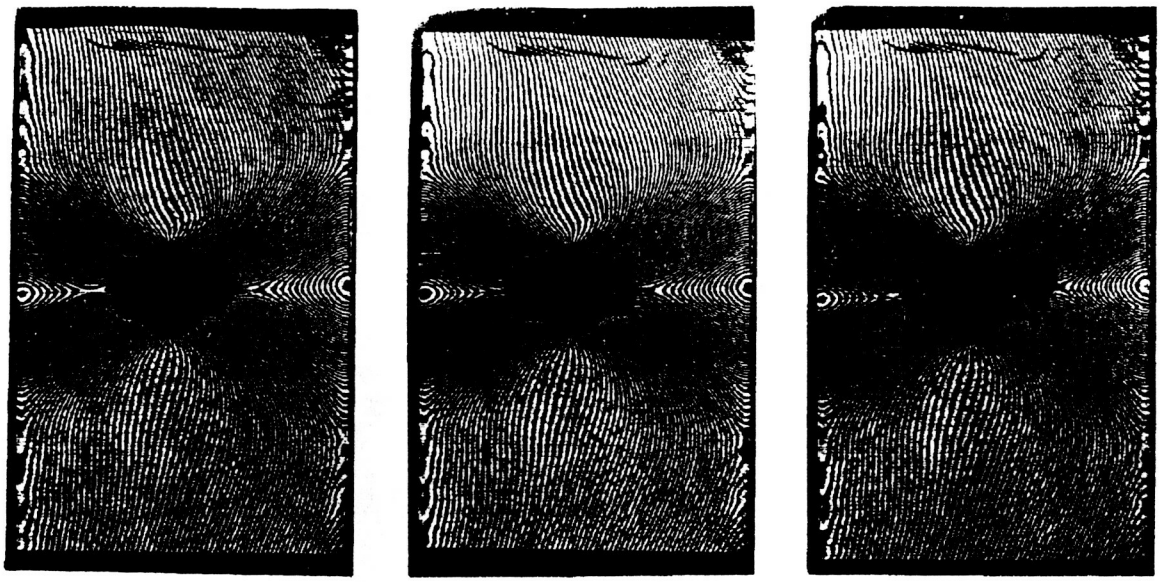

TIME = 1 MIN TIME = 10 MIN TIME = 30 MIN

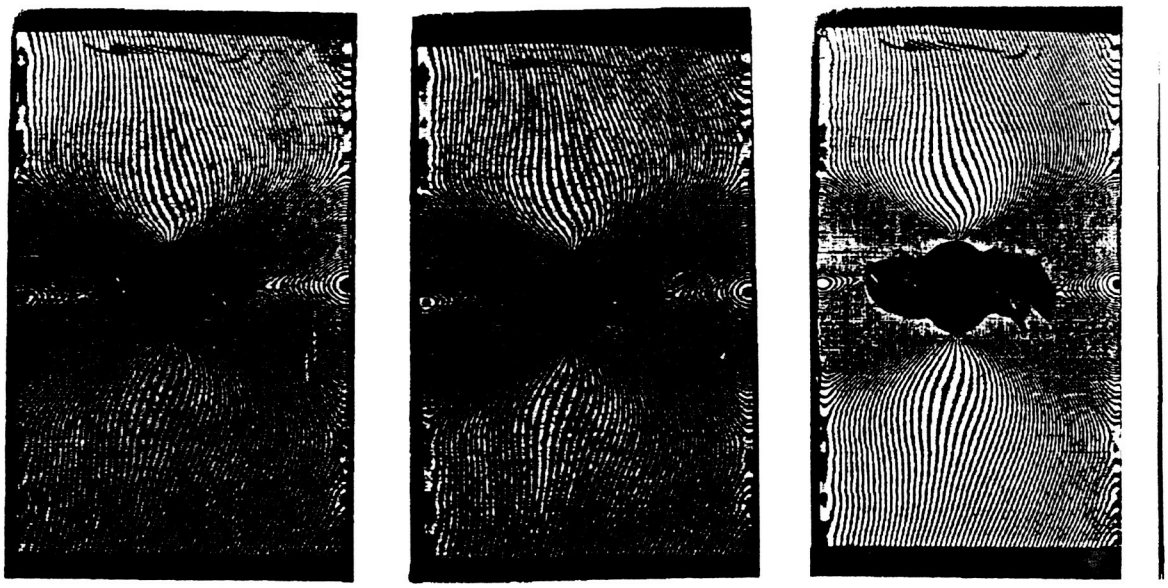

TIME = 1 HRS TIME = 5 HRS TIME = 10 HRS

Figure 35: Delamination of Type D $[90/45/90/-45]_{6s}$ Gr/Ep U-displacement

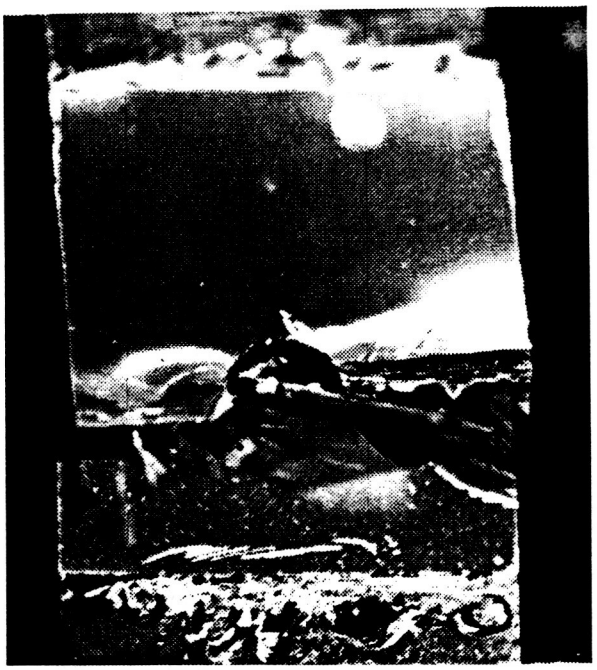

Figure 36: Front View of Failed $[90°/-45°/90°/45°]_{6s}$ Gr/Ep Specimen.

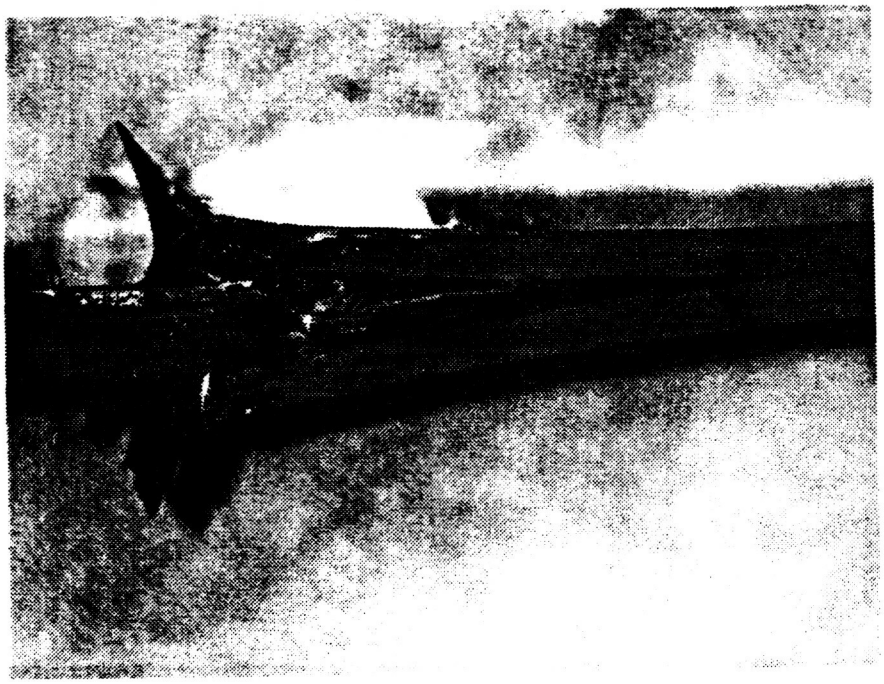

Figure 37: Side View of Failed $[90°/-45°/90°/45°]_{6s}$ Gr/Ep Specimen.

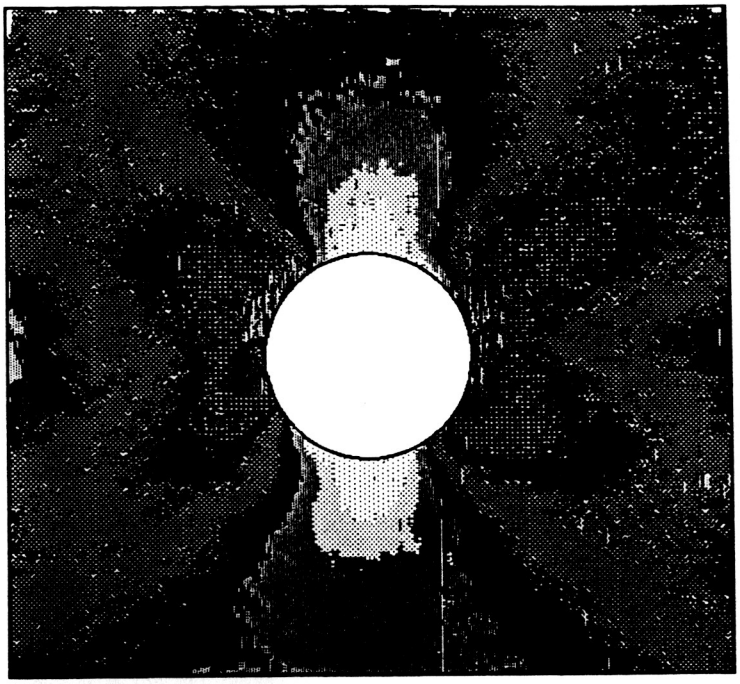

Figure 38: Axial Strain Field Map $[90/-45/90/45]_{6s}$, t = 1 min
(Compressive Strains)

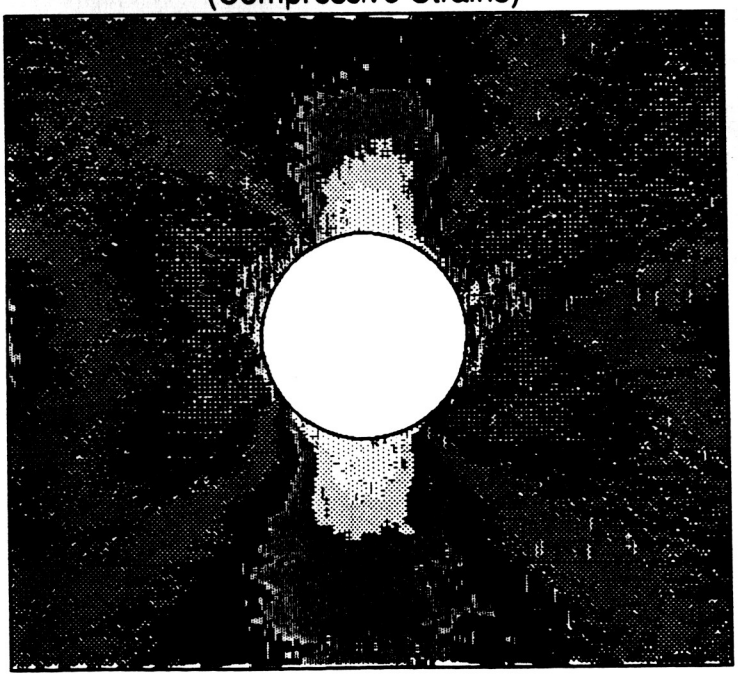

Figure 39: Axial Strain Field Map $[90/-45/90/45]_{6s}$, t = 10 hrs
(Compressive Strains)

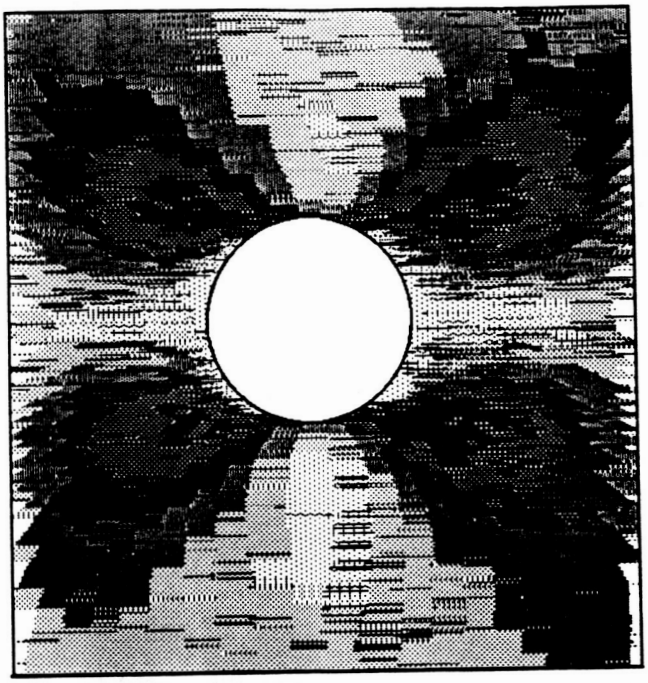

Figure 40: Transverse Strain Field Map $[90/-45/90/45]_{6s}$, t = 1 min (Tensile Strains)

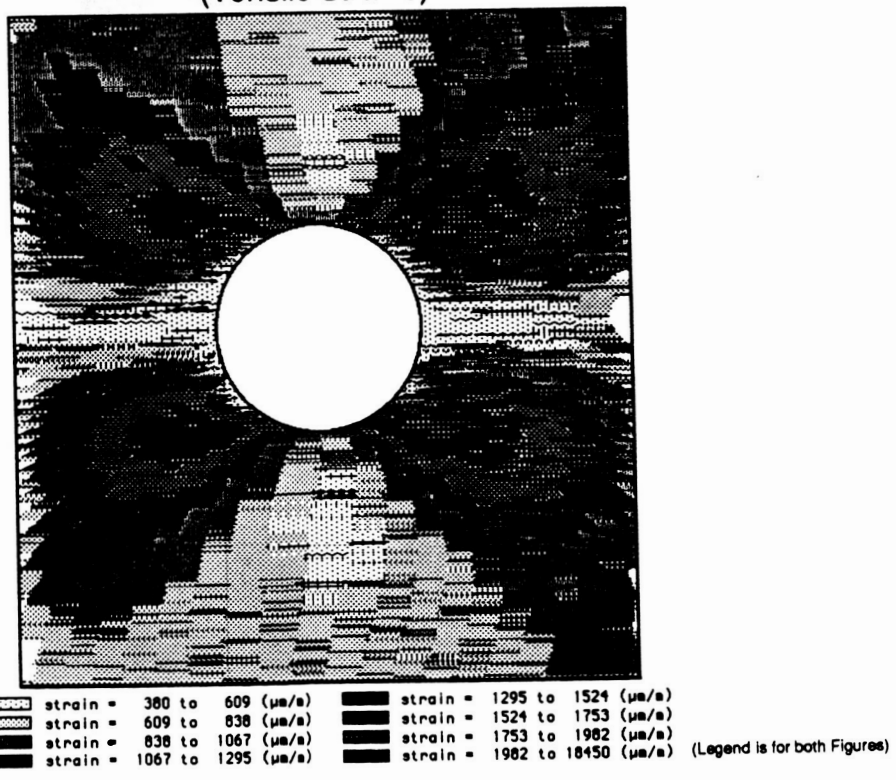

Figure 41: Transverse Strain Field Map $[90/-45/90/45]_{6s}$, t = 10 hrs (Tensile Strains)

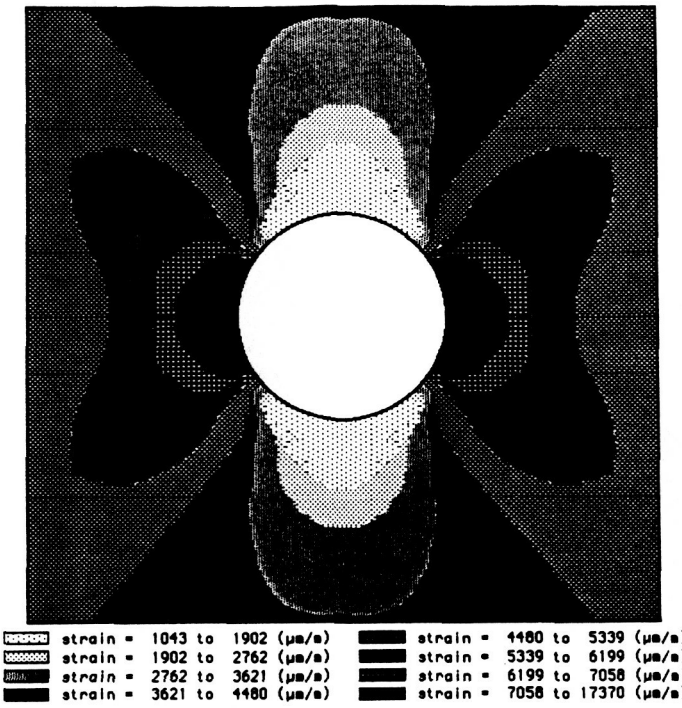

Figure 42: F.E. Axial Strain Field Map $[90/-45/90/45]_{6s}$
(Compressive Strains +)

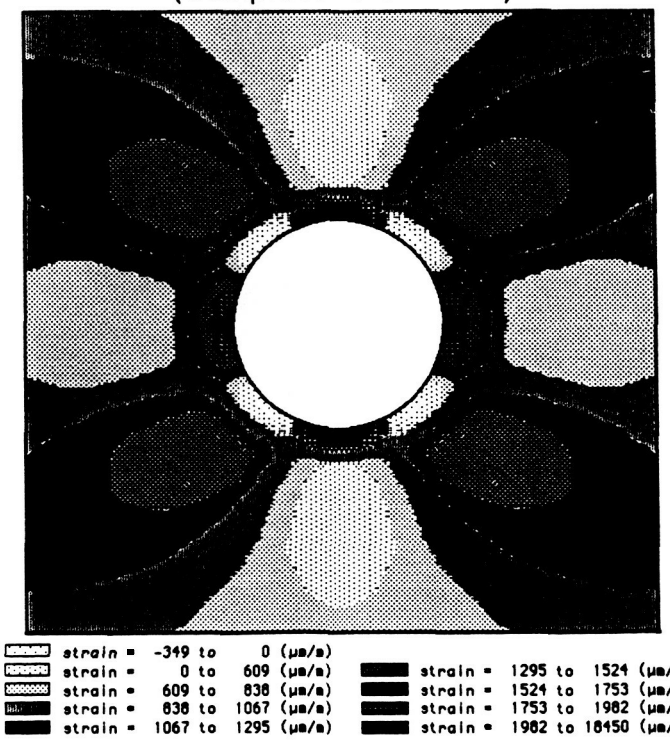

Figure 43: F.E. Transverse Strain Field Map $[90/-45/90/45]_{6s}$
(Tensile Strains +)

Graphite/PEEK Specimens with holes

The Gr/PEEK specimens tested were quasi-isotropic Type E: $[45/0/-45/90]_{6s}$. The four specimens tested contained holes of the following diameters; 1.58 mm, 3.17 mm, 6.35 mm and 9.52 mm. The stress levels of the test were: -335 MPa (-48,588 psi), corresponding to 77% of the ultimate strength; -302 MPa (-43,800 psi), corresponding to 69% of the ultimate strength; -308 MPa (-44,671 psi), corresponding to 93% of the ultimate strength; and -238 MPa (-34,518 psi), corresponding to 63% of the ultimate strength; respectively. No viscoelastic response was found in either the axial or transverse strain distributions for any of the four Gr/PEEK specimens tested, and therefore only the 1 min strain fields will be presented.

The axial strain field maps are presented in Figures 44 through 47. The axial strain field for the specimen with a 1.58 mm dia hole (Figure 44) shows a near uniform strain field in a significant portion of the test area. The axial strain field for the 3.17 mm dia hole specimen (Figure 45) shows the familiar "wing" shaped strain regions found in the other specimens. The disturbances generated by the hole extend further from the center of the strain field. The 6.35 mm hole specimen shows an axial strain field (Figure 46) similar to those of the 6.35 mm hole Gr/Ep specimens. The disruptions in the strain field, in the familiar "winged" shaped regions, are much more extensive than in the specimens with

smaller holes. The disturbances extend throughout the entire gage area of the specimen.

The axial strain field map for the specimen with a 9.52 dia hole is presented in Figure 47. The strain field shows some of the "wing" shaped strain regions, however, most of the strain patterns extend out past the gage area to the edge of the specimen where they combine with effects produced by the edge of the specimen.

The transverse strain fields are presented in Figures 48 through 51. The 1.58 mm dia hole specimen transverse strain field (Figure 48) shows large portions of uniform strain. The outer edges of the gage area show almost no effects from the hole. The general shape of the strain field near the hole however, is similar to the strain fields found in the other specimens. Small "looping" regions of strain emanate on ±45° diagonals from the hole. The transverse strain fields for the 3.17 mm dia hole specimen (Figure 49) shows an increase in these "looping" regions. The diagonal direction loops in the 6.35 mm dia hole specimen (Figure 50) have extended to the corners of the gage area. It is also interesting to note how the edge effects have further combined with effects from the hole. The general shape of the transverse strain, like the axial strain field for this specimen, is similar to the shapes found in the Gr/Ep specimens. The transverse strain field map for the 9.52 mm dia hole specimen is presented in Figure 51. The "looping" strain regions are very apparent in this specimen. Several areas of the strain field display regions where a strain pattern extends away

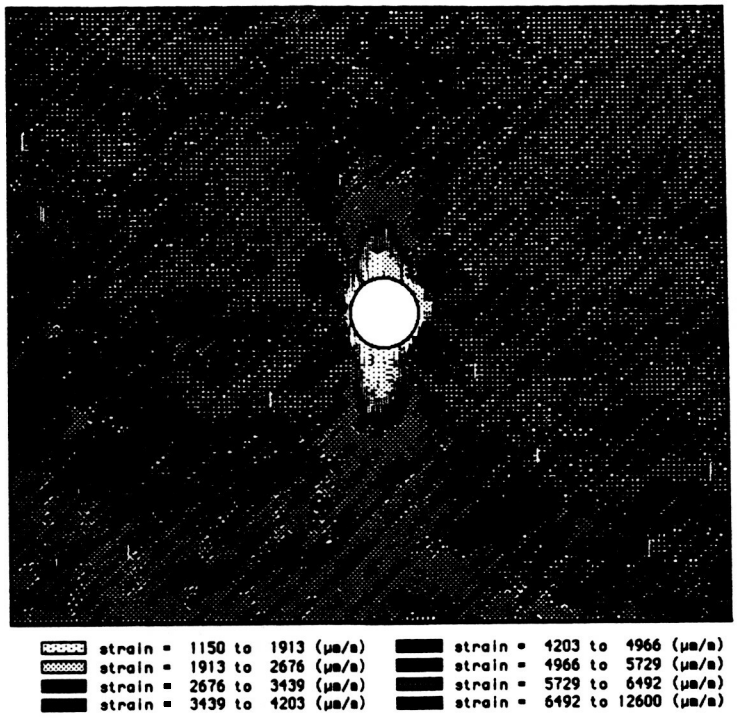

Figure 44: Axial Strain Field Map, 1/16" dia hole Gr/PEEK, t = 1 min
(Compressive Strains)

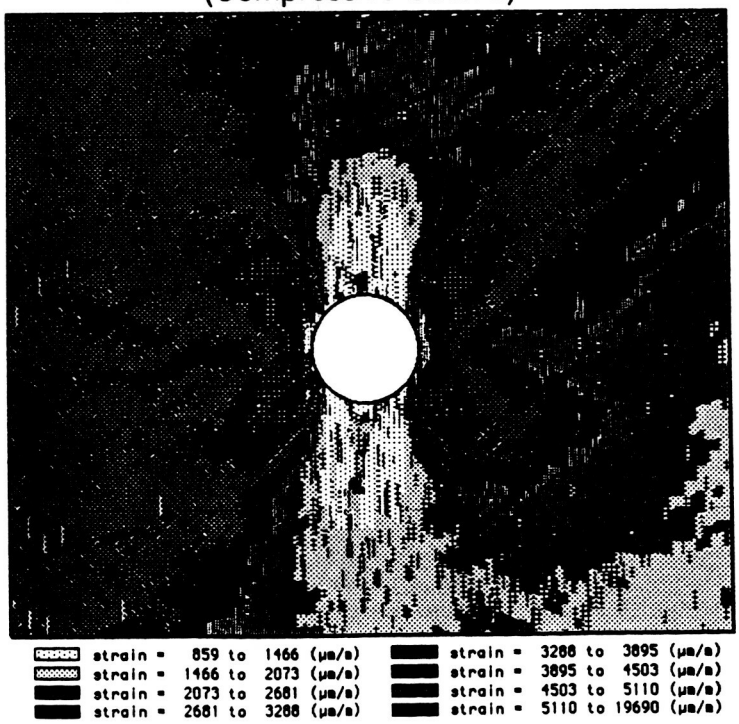

Figure 45: Axial Strain Field Map, 1/8" dia hole Gr/PEEK, t = 1 min
(Compressive Strains)

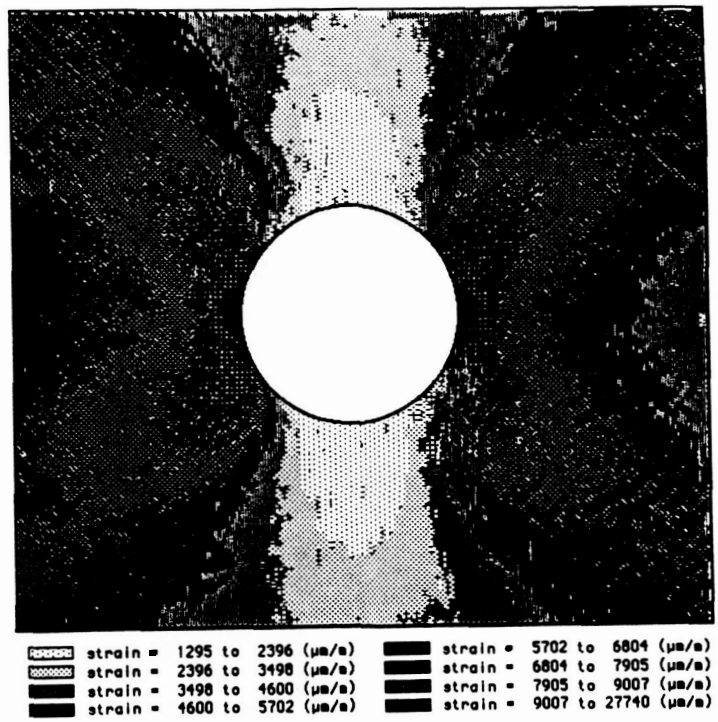

Figure 46: Axial Strain Field Map, 1/4" dia hole Gr/PEEK, t = 1 min
(Compressive Strains)

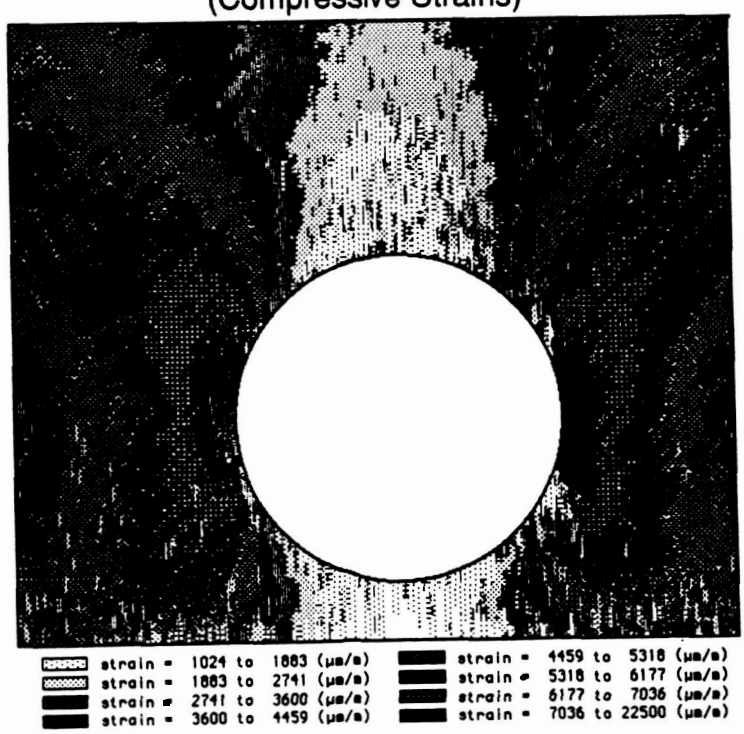

Figure 47: Axial Strain Field Map, 3/8" dia hole Gr/PEEK, t = 1 min
(Compressive Strains)

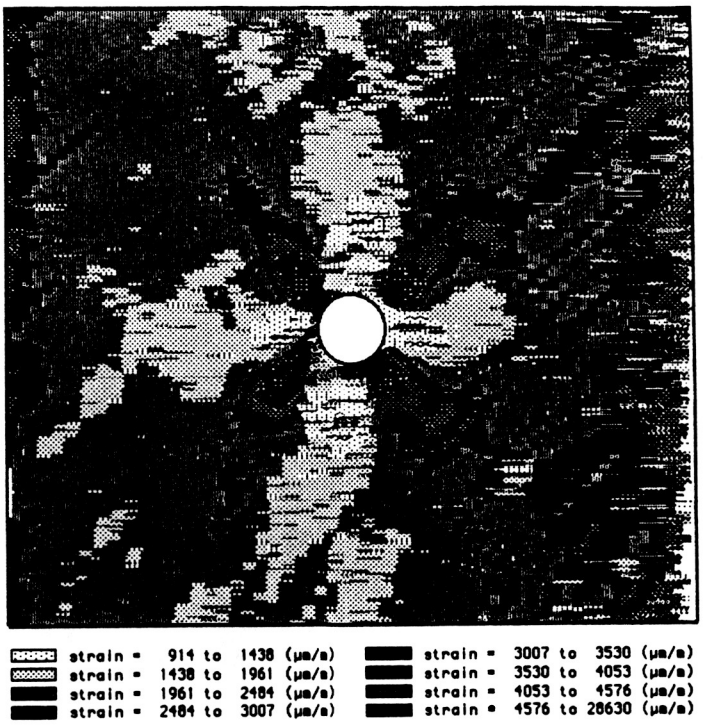

Figure 48: Transverse Strain Field Map, 1/16" dia hole Gr/PEEK, t = 1 min (Tensile Strains)

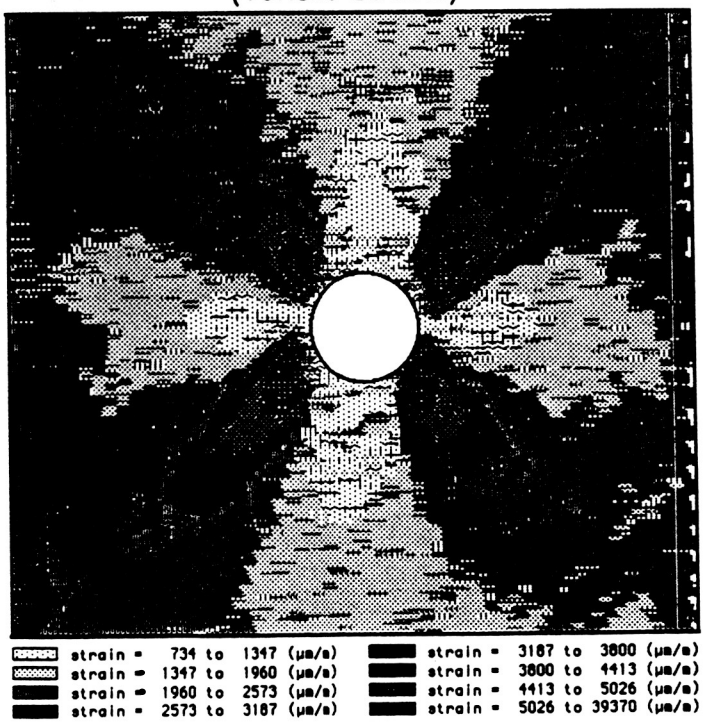

Figure 49: Transverse Strain Field Map, 1/8" dia hole Gr/PEEK, t = 1 min (Tensile Strains)

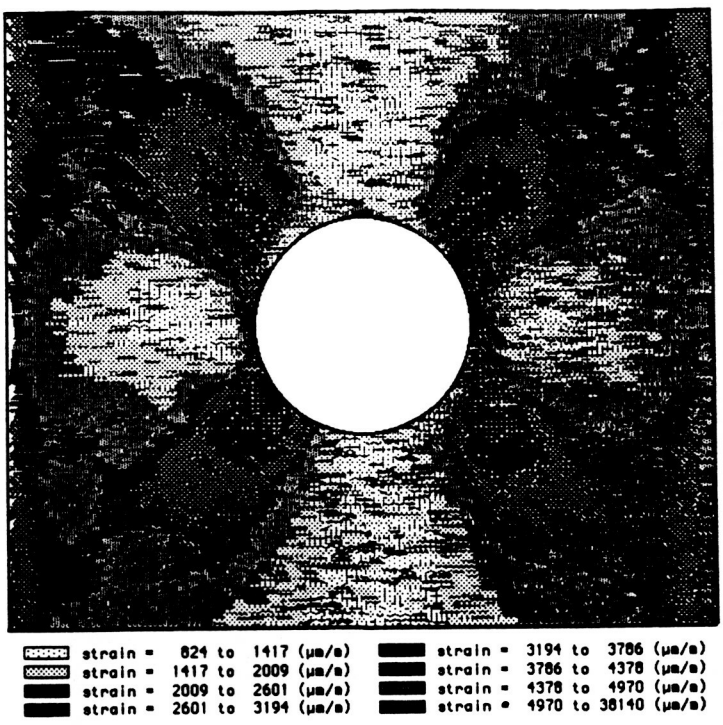

Figure 50: Transverse Strain Field Map, 1/4" dia hole Gr/PEEK, t = 1 min (Tensile Strains)

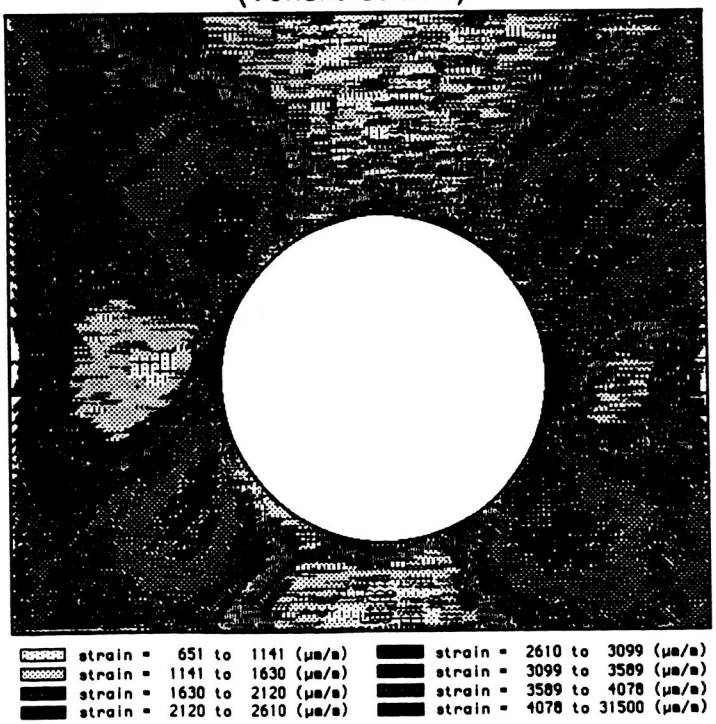

Figure 51: Transverse Strain Field Map, 3/8" dia hole Gr/PEEK, t = 1 min (Tensile Strains)

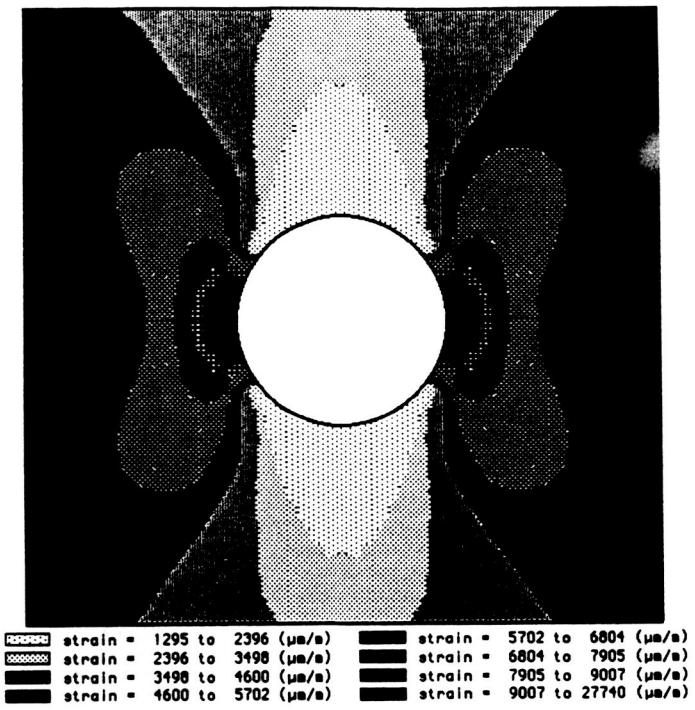

Figure 52: F.E. Axial Strain Field Map, 1/4" dia hole Gr/PEEK
(Compressive Strains +)

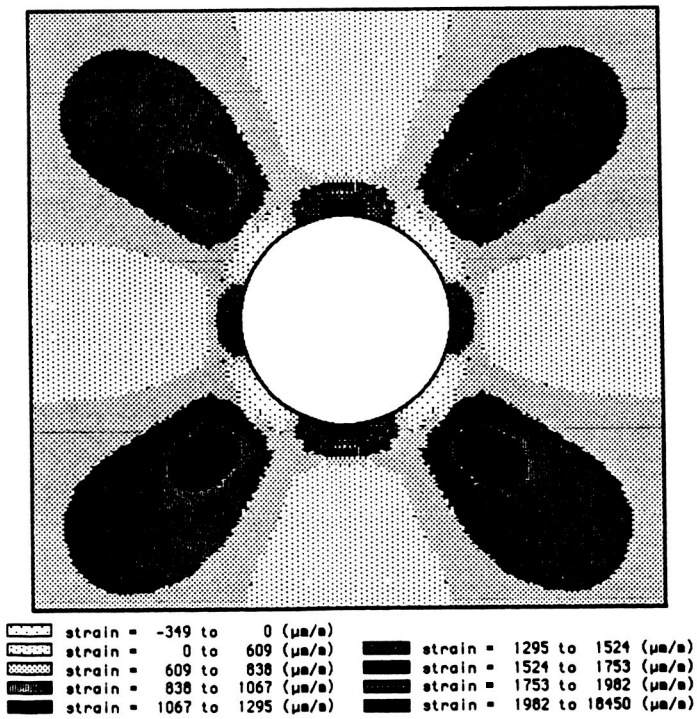

Figure 53: F.E. Transverse Strain Field Map, 1/4" dia hole Gr/PEEK
(Tensile Strains +)

from the hole and then "loops" back on itself, ending where it originated.

A finite-element analysis was performed for the 6.35 mm dia hole specimen using the following material properties reported by Tsai[30]:

E_{11} = 134 GPa

E_{22} = 8.9 GPa

G_{12} = 5.1 GPa

A value of ν_{12} = 0.28 was reported by Tsai for Gr/PEEK in tension. Since ν_{12} has been found to be significantly higher in compression, than in tension for other composite systems, a value of ν_{12} = 0.5 was arbitrarily selected for use in the finite-element analysis. Comparison of the finite-element strain fields (Figures 52 and 53) with the experimentally measured strain fields (Figures 44 and 48) shows a good correlation between the two.

SUMMARY, CONCLUSIONS AND RECOMMENDATIONS

Summary

The overall goal of this study was to measure elastic and viscoelastic strain fields induced in composite laminates by compressive loading. Moiré interferometry was used to produce moiré fringe patterns for the u- and v-displacement fields. A computer based data reduction system was developed which, using a digitized image of the u- and v-displacement field, produced a whole field strain field map for both the transverse and axial strain fields. It would also be possible to use a similar approach to produce a shear strain field map, although this was not attempted in this study. These strain field maps allowed for comparison of strain distributions at different times. A comparison was made for strain fields of different composite material layups and also for strain fields in composites specimens with different size holes. Solid specimens were tested and the average strain computed using the computer data reduction system. These strains were then used to determine fundamental engineering moduli. Measured strain distributions for specimens with holes were compared with predictions obtained using finite-element techniques.

Conclusions

Strain Field Map

The strain field map proved to be a valuable tool in the analysis of strain distributions. Comparisons of different material layups showed distinctly different stain fields. The irregularities that appeared in the strain fields did not mask the overall shape of the strain fields, so analysis and comparisons could still be made. The "irregularities" in the experimentally measured strain distributions might at first be interpreted as "noise" or "scatter" in the data. While a percentage of these irregularities is undoubtedly due to experimental error, the authors are convinced that a significant fraction of this scatter is, in fact, an accurate representation of the surface strains. That is, the "scatter" in strain is simply a reflection of the inherent heterogeneity of composites. This is supported by the results of Post and others[6], where composite specimens subjected to tensile loadings have exhibited irregularities in surface strains as high as ±15%. The nonuniformity in surface strain distributions tend to cause irregularities in the strain contour maps presented herein. Note that the finite-element analysis does not account for the possibility of inhomogeneities, and hence the strain contours prepared using finite-element results indicate very smooth and well-defined strain contours.

It is important to note once again that the data reduction scheme used in this analysis measures magnitudes of strain. The

$[0]_{48}$ transverse displacement field showed two "islands" of compressive strain in a predominantly tensile field. The data reduction method does not identify the algebraic sign of strain. The responsibility falls on the user to identify any regions where sign changes may occur. The strain fields analyzed in this study were relatively simple, so this could be done easily. However, if complex strain fields are to be analyzed using this approach, a more rigorous determination of actual fringe number is required.

Viscoelastic Effects

Viscoelastic effects were noted in two of the specimens containing holes. The matrix dominated layups, $[90]_{48}$ and $[90/-45/90/45]_{6s}$, showed mild viscoelastic response over the length of the test when subjected to stress levels of about 33% and 45% of the static ultimate strength, respectively. Major time dependent effects were seen in a $[90/-45/90/45]_{6s}$ specimen with hole subjected to a creep load of -308 MPa, or about 90% of the static ultimate strength. This specimen delaminated immediately upon application of the load, and the delaminated region grew until complete catastrophic failure occurred at about 16 hours after application of the load. In this case the response is a complex combination of both viscoelastic and fracture mechanisms.

With the exception of the $[90/-45/90/45]_{6s}$ specimen which failed catastrophically after 16 hrs, the viscoelastic effects observed during this study were relatively mild. Note, however, that the measurements were obtained over a 10-hr period and at room

temperatures. The implication is that at much longer times (say after weeks, month, or years) the composite laminates considered in the study may exhibit very significant viscoelastic deformation, which may be accompanied by delaminations and eventually catastrophic failure.

It is believed that the (nominal) 10-hr creep test time used in this study is "about" as long in duration as can be conveniently performed using moiré interferometry. Hence, if truely long-term effects are to be investigated using moiré interferometry, the effects due to viscoelastic behavior must be "accelerated" in some fashion. A recommendation for further study is use of the present moiré system under conditions of moderately elevated temperatures (say 90°C, or about 200°F).

Comparison Between Experimental and Finite-Element Results

The finite-element results compare well in most cases with the experimental results. However, in general the finite-element strain field maps indicate lower strain in areas removed from the hole and higher strain in areas close to the hole. It is hypothesized that the high stress levels at the edge of the hole induced nonlinear material behavior at these points. This nonlinear behavior may arise from the formation of localized micro-cracks or voids. These micro failures in the vicinity of the hole would result in a redistribution of strain. This redistribution may result in slightly lower strains

immediately adjacent to the hole and slightly higher strains throughout the rest of the strain field, which agrees in a qualitative sense with the results obtained.

Overall Conclusions regarding the Use of Moiré Interferometry

To the author's knowledge, this program represents the first time that moiré interferometry has been used under creep conditions. Overall, the use of moiré interferometry has been very successful. The moiré system developed has proven to be stable and suitable for use during creep periods up to 24 hrs in duration. It is not clear if the system would remain stable for much longer times, say for several days or weeks. It has been possible to identify slight viscoelastic deformations which occur at room temperatures in composite laminates through the use of moiré. It is not likely that other popular strain measurement devices such as resistance foil strain gages would have been stable enough to have identified this behavior.

Moiré interferometry itself is a powerful tool for use in studying composites. An outstanding advantage of moiré is the ability to obtain whole field displacements and/or strains, as opposed to point-measurement techniques such as strain gages, extensometers, or LVDT's. Furthermore, moiré interferometry can be configured so as to obtain measurements with a sensitivity which equals or exceeds those available with other techniques.

On the other hand, moiré interferometry is an exacting technique. Specimen and grating preparation techniques, as well as subsequent bonding of the grating to the specimen, are considerably more involved than those associated with bonding strain gages, for example. The personnel involved in this study have found that as more experience was gained, much better moiré patterns were obtained. These improvements occurred even though no apparent changes in procedure were implemented. In other words, considerable expertise is required before high-quality moiré patterns can be obtained by the researcher. This expertise can only be gained through personal experience in the lab. The exacting nature of moiré interferometry has definite practical implications. For example, in most experimental studies involving the use of strain gages several repeated tests, over a wide range of test conditions, will normally be performed. Very few repeated tests were performed during this study, and the range of test conditions was more limited than might otherwise be desired. These aspects of the program were required by the combination of time and budget constraints and the degree of difficulty in performing each moiré test.

Recommendations

Moiré Fixture

The Moiré fixture could be improved with additional alignment features, which would insure the specimen face was perpendicular

to the incoming light and centered in the loading frame. The ability to use multiple frequencies of virtual gratings would also aid in the examination of high strain fields. In applications such as the matrix dominated layups, a different frequency of grating for the transverse and axial strains would greatly improve the analysis of these strain fields. This may be achieved using the recently-developed "composite" specimen gratings described by Wang, Kang and Kobayashi[32].

Elevated Temperature/Humidities Testing

Viscoelastic response was seen in some of the specimens tested. It would be of great interest to expose the specimens to a more aggressive environment such as elevated temperatures and humidities where viscoelastic effects are likely to over a convenient test period. This type of testing would allow for viscoelastic analysis of any material layup such as the "fiber-dominated" layups which do not show any viscoelastic response at short times and at ambient conditions.

Elevated temperature/humidity testing would require additional apparatus in the form of an environmental chamber to fit around the compression and/or moiré fixture. However, the compression fixture and moiré system developed during this study were designed with eventual inclusion of an environmental chamber in mind. Hence, the inclusion of a chamber in the existing test setup can be achieved with relative ease.

Data Reduction System

The data reduction system developed during this study resulted in generally good results. However when moiré fringe patterns of low quality were obtained, i.e., excessive noise was present, the resulting strain fields also showed areas of noise. Solutions for this are of two types. Either obtain consistently "clean" moiré patterns, or develop a computer-based filtering system which would allow for a numerical filtering of (digitized) "noisy" moiré patterns to obtain clean patterns. Potential methods of numerical filtering of the digitized moiré patterns were briefly evaluated during this study, but a satisfactory system has not yet been developed. Numerical filtering should be possible, however, and is recommended as an area of further study.

As previously mentioned, as experience is gained by the individual the quality of moiré patterns obtained by that person generally improves. Hence, the only way of obtaining consistently "good" moiré patterns is the development of personal experience.

A second area of improvement is in calculation of strain values. In the present effort strains were determined using a simple averaging scheme which approximates the derivative of a displacement field. An improvement would be to incorporate a more sophisticated numerical differentiation scheme, such as the use of Lagragian polynomials.

REFERENCES

1) Jones, Robert M. Mechanics of Composite Materials. Scripta Book Co., (1975).

2) Post, D. "Moiré Interferometry at VPI & SU." Experimental Mechanics, Vol 23, No. 2 (June 1983), 203-210.

3) McDonach, A., McKlelvie, J., and Walker, C. A., "Stress Analysis of Fibrous Composites Using Moiré Interferometry." Optics and Lasers in Engineering, Vol 1 (1980), 85-105.

4) Post, D. "Moiré Interferometry for Damage Analysis of Composites." Experimental Techniques, Vol 7, No. 1 (July 1983), 17-20.

5) Bowles, D.E., Post, D., Herakovich, C. T., and Tenney, D. R. "Moiré Interferometry for Thermal Expansion of Composites." Experimental Mechanics, Vol 21, No. 12 (Dec 1981), 441-447.

6) Post, D., Czarnek, R., and Joh, D. "Shear Strains in a Graphite-PEEK Beam by Moiré Interferometry with Carrier Fringes." Proc. of the 1986 SEM Fall Conference on Experimental Mechanics. (Nov 1986), 159-164.

7) Dadkhah, M. S., Wang, F. X., and Kobayashi, A. S. "Simultaneous on Line Measurement of Orthoganal Displacement Fields by Moiré Interferometry." Experimental Techniques. (to be published 1988).

8) Dadkhah, M. S., Wang, F. X., and Kobayashi, A. S. "J-Integral Measurement Using Moiré Interferometry". VI International congress of Experimental Mechanics. (to be published June 1988).

9) Dadkhah, M. S. "Ductile Fracture Under Complex Loading Utilizing Moiré Interferometry." Ph. D Dissertation, Dept. of Mech. Engr., University of Washington, (1988).

10) Kang, B. S. -J, and Kobayashi A. S. "J-Resistance Curves in Aluminum SEN Specimens." Experimental Mechanics, (to be published 1988).

11) Kang, B. S. -J, Kobayashi A. S., and Post, D. "Stable Crack Growth in Aluminum Tensile Specimens." Experimental Mechanics, Vol 27, No. 3 (Sept 1987), 234-245.

12) Klein, R. J. "Strain Measurement in Composites Subjected to Compressive Loading Using Moiré Interferometry." M.S. Thesis, Dept. of Mech. Engr., University of Washington, (1986).

13) Klein, R. J., and Tuttle, M. E. "Strain Measurement in Composites Subjected to Compressive Loading Using Moiré Interferometry." Proc. 1987 SEM Spring Confrence on Experimental Mechanics, (1987)

14) Klein, R. J., and Tuttle, M. E. "Strain Measurement in Composites Subjected to Compressive Loading Using Moiré Interferometry." Proc. 31st Ann. SPIE Int'nl Tech. Sym. on Optical and Optoelectronic Appl. Science and Tech., 16-21 August, San Diego Ca.

15) Clark, R. K., and Lisagor, W. B. "Compression Testing of Graphite/Epoxy Composite Materials." ASTM STP 734 (1981), 34-53.

16) Post, D. and Baracat, W. A. "High-Sensitivity Moiré Interferometry a Simplified Approach." Experimental Mechanics, Vol 21, No. 3 (March 1981), 100-104.

17) Post, D. "Moiré Interferometry." Chpt 7 in Handbook on Experimental Mechanics. A.S. Kobayashi Ed. Englewood Cliffs: Prentice Hall, (1987), 314-387.

18) Herrera-Franco, P.J. and Cloud, G.L. "Moiré Study of Mechanically Fastened Composites." Proc. 1985 SEM Spring Conference on Experimental Mechanics, (1985), 149-152.

19) Basehore, M. L. and Post, D. "High-frequency, High-reflectance Transferable Moiré Gratings." Experimental Techniques, Vol 8, No. 5 (May 1984), 29-31.

20) "Surface Preparation for Strain Gage Bonding." Micro-Measurements Instruction Bulletin B-129-4, Measurement Group, Inc., Raleigh, N.C.

21) Miyano, Y., Kanemitsu, M., Kunio, T., and Kuhn, H. A. "Role of Matrix Resin on Fracture Strengths of Unidirectional CFRP." Journal of Composite Materials, Vol 20, (1986), 520-538.

22) Gilbert, J. A., Dudderar, T. D., Matthys, D. R., Johnson, H. S. and Franzel, R. A. "Two-Dimensional Stress Analysis Combining High-Frequency Moiré Measurements with Finite-Element Modeling." Experimental Techniques, Vol , No. (March 1987), 24-28.

23) Kobayashi, A. S. "Hybrid Experimental-Numerical Stress Analysis." Experimental Mechanics, Vol 23, No. 3 (Sept 1983), 338-347.

24) Dally, J W. and Riley, W. F. Experimental Stress Analysis. McGraw-Hill Book Co., (1978).

25) Weissman, E. M. and Post, D. "Full-Field Displacement and Strain Rosettes by Moiré Interferometry." Experimental Mechanics, Vol 22, No. 9 (Sept 1982), 324-328.

26) Wasowski, J. J. and Wasowski, L. M. "Computer-Based Optical Differentiation of Fringe Patterns." Experimental Techniques, Vol 11, No. 4 (March 1987), 16-18.

27) Asundi, A. and Cheung, M.T., "Moiré Interferometry." Experimental Techniques, Vol 11, No. 8 (August 1987), 28-30.

28) Halpin, J. C., Primer on Composite Materials: Analysis, Revised Edition, Technomic Pub. Co., (1984).

29) Tsai, S. W. Composite Design, 3rd Edition, Think Composites (Publisher), (1987). Program MIC-MAC, available from the same source.

30) Smith, C. W. "Exp. Fracture Mechanics." Chpt 20 in Handbook on Experimental Mechanics. A.S. Kobayashi Ed. Englewood Cliffs: Prentice Hall, (1987), 891-956.

31) Carlsson, L. "Interlaminar Stress at a Hole in a Composite Member Subjected to In-Plane Loading." Journal of Composite Materials, Vol 17 (1983), 238-249.

32) Wang, F. X., Kang, B. S. -J. and Kobayashi, A. S. "A Composite Grating For Moiré Interferometry." Proc. 31st Ann. SPIE Int'nl Tech. Sym. on Optical and Optoelectronic Appl. Science and Tech., 16-21 August, San Diego Ca.

APPENDIX A:COMPUTER PROGRAMS

Two FORTRAN-based computer programs were developed in-house during this program; programs MOIRE and STRREG. These programs allowed the calculation of strains from digitized moiré fringe patterns, and subsequent display of strain contour plots. Listing of the source code for each of these programs is listed below.

Program MOIRE

```
      implicit none
      integer*2 data(6)
      integer*2 width,height
      integer*1 pic(400)
      integer*1 testbyte,testnum
      real df,scale,evencheck
      real str(1000)
      character*1 pix(8)
      integer lsf,rsf,tof,bof,colf,coll
      real
fringe(1000),ddymin,ddymax,ddxmin,ddxmax,tstr,avestr,rcnt
      integer resp,cnt
      character filename*64
      integer*1 offset

      integer i,k,j,n,l,m,scancolm,scanline,row,col,fileloc,byte
      integer sec

      character*1 pixel(8,3000)

      tstr = 0.0
      cnt = 0
```

```
      ddxmin = 1.0
      ddxmax = -1.0


      ddymin = 1.0
      ddymax = -1.0


* Open the file.  Bitmap data is binary, so use unformatted access.

      write(9,*)'Input the file to be scanned'
      read(9,500)filename
500   format(A)

      open(unit=20, FILE=filename, STATUS='old',ACCESS='direct',
     + FORM='unformatted',RECL=2)

      write(9,501)
501   format(1x,'Choose the desired analysis',
     + /1x,'1.  Calculation of du/dx',
       + /1x,'2.  Calculation of dv/dy',/1x)
      read(9,*)resp

      write(9,*)'Input the scale.  (Pixels/In).'
      read(9,*)scale

      write(9,*)''
      write(9,*)'Input the reference grating frequency.  (l/mm)'
      read(9,*)df

      df = 1.0/(df*25.4)

      write(9,*)'reading the moiré picture'
*
* read file info
*
      do(i=1,6)
      read(unit=20,REC=i)data(i)
      repeat
      close(20)
```

```
      width = data(4)
      height = data(5)

      write(9,*)'scanning resolution   ',data(1)
      write(9,*)'scanning width        ',8*data(4)
      write(9,*)'scanning height       ',data(5)
      write(9,*)'  '
*
* This block checks to see if the scanning width is even or odd
* If the width is even an extra byte is added to each record in the
* scanned file, so this must be compenstated for here.
*


      evencheck = width/2.0
      evencheck = evencheck - (width/2)
      if(evencheck.EQ..5)then
            offset = 3
      else
            offset = 4
      endif

*
* This block inserts the data into a screen size array
*

      IF(resp.EQ.1)THEN

      open(unit=10,file='ddx.output',status='new')

      do(scanline = 40,height,8)

      sec = (scanline - 1 + 8)/8

      write(9,*)'Scanning Section # ',sec

      open(unit=20, FILE=filename, STATUS='old',ACCESS='direct',
     + FORM='unformatted',RECL=1)
```

```
      do(row = 4,8,4)

      fileloc=(row-1+scanline-1)*(width+offset)+513
      do(byte=fileloc,fileloc+width+offset)
      i=byte-fileloc+1
      read(unit=20,rec=byte,end=200)pic(i)
      repeat

200   do(i=1,width)
      k = i + 4
      if(pic(k).LT.0)then
            pix(1) = 'B'
      else
            pix(1) = 'W'
      endif
      scancolm = ((i*8)-7)
      pixel(row,scancolm) = pix(1)
      testnum = 64;

      do(j=2,8)

       testbyte = pic(k).and.testnum
      if(testbyte.NE.0)then
            pix(j) = 'B'
      else
            pix(j) = 'W'
      endif
      testnum = testnum/2
      scancolm = ((i*8)-8+j)
      pixel(row,scancolm)=pix(j)
      repeat
      repeat
      repeat

      close(20)
```

```
      CALL
DDX(width,height,pixel,scale,df,ddxmin,ddxmax,sec,tstr,cnt)

      repeat

      ELSEIF(resp.EQ.2)then


      open(unit=12,file='ddy.output',status='new')

      do(sec = 1,width)

      write(9,*)'Scanning Section # ',sec

      open(unit=20, FILE=filename, STATUS='old',ACCESS='direct',
     + FORM='unformatted',RECL=1)

      do(row = 40,height)

      fileloc=(512+offset)+(sec-1)+(row-1)*(width+offset)

      byte=fileloc
      read(unit=20,rec=byte,end=210)pic(1)

210   if(pic(1).LT.0)then
            pix(1) = 'B'
      else
            pix(1) = 'W'
      endif
      scancolm = (1)
      pixel(scancolm,row) = pix(1)
      testnum = 64;

      do(j=2,8)

        testbyte = pic(1).and.testnum
      if(testbyte.NE.0)then
            pix(j) = 'B'
      else
            pix(j) = 'W'
```

```
      endif
      testnum = testnum/2
      scancolm = (j)
      pixel(scancolm,row)=pix(j)
      repeat
      repeat

      close(20)

      CALL
DDY(width,height,pixel,scale,df,ddymin,ddymax,sec,tstr,cnt)

      repeat

      else
      endif

      rcnt = cnt
      avestr = tstr/rcnt

      open(unit=14,file='maxmin.out',status='new')

      if(resp.EQ.1)then
         write(14,510)ddxmin,ddxmax,avestr
510   format(1x,e16.8,/1x,e16.8,/1x,e16.8)
      close(14)

      else
         write(14,530)ddymin,ddymax,avestr
530   format(1x,e16.8,/1x,e16.8,/1x,e16.8)
      close(14)

      endif


      WRITE(9,*)'DONE'
      READ(9,*)
      END
```

```
      SUBROUTINE
DDX(width,height,pixel,scale,df,ddxmin,ddxmax,sec,
     .  tstr,cnt)

      real  scale,df
      integer*2  width,height
      character*1  pixel(8,3000)
      integer  lsf,rsf,tof,bof,colf,coll
      real  ddxmin,ddxmax,str(1000)
      real  fringe(1000),ddymin,ddymax,tstr
      character  filename*64
      integer  i,k,j,n,l,m,sec,cnt

*  calculation  of  x-fringe  locations

      write(9,*)'Calculating  x-fringe  locations  and  ddx'

      width  =  width*8

      do(i=4,8,4)

        do(k=1,1000)
          fringe(k) = 0.0
        repeat

        lsf = 0
        rsf = 0
        n = 1

         do(j=1,width)
           if(pixel(i,j).EQ.'B'.AND.lsf.EQ.0)then
            lsf = j
           elseif(pixel(i,j).EQ.'W'.AND.lsf.NE.0)then
            rsf = j-1
              fringe(n) = (rsf+lsf)/2.0
          n = n+1
           lsf = 0
           rsf = 0
         else
         endif
```

```
        repeat
*
* calculation of d/dx
*
       n = 2
100     if(fringe(n+1).NE.0)then
           str(n) = (2.0*df*scale)/(fringe(n+1)-fringe(n-1))
          if(str(n).LT.ddxmin)ddxmin = str(n)
          if(str(n).GT.ddxmax)ddxmax = str(n)
         n = n+1
         goto 100
        else
        endif

      m = (sec*8-8)+i


      do(k=2,n-1)

           write(10,500)fringe(k),m,str(k)
        tstr = tstr + str(k)
       cnt = cnt + 1

      repeat

500   format(1x,f6.1,2x,i5,2x,e16.8)

      repeat


      width = width/8

      RETURN
      END


      SUBROUTINE
DDY(width,height,pixel,scale,df,ddymin,ddymax,sec,
     . tstr,cnt)
```

```
      integer*2  width,height
      character*1  pixel(8,3000)
      integer  lsf,rsf,tof,bof,colf,coll
      real  df,scale
      real  ddxmin,ddxmax,str(1000)
      real  fringe(1000),ddymin,ddymax,tstr
      character  filename*64
      integer  i,k,j,n,l,m,sec,cnt

*  calculation  of  y-fringe  locations

      write(9,*)'Calculating  y-fringe  locations  and  ddy'

      width  =  width*8

      do(j=4,8,4)

        do(k=1,1000)
          fringe(k) = 0.0
        repeat

        tof = 0
        bof = 0
        n = 1

        do(i=1,height)
          if(pixel(j,i).EQ.'B'.AND.tof.EQ.0)then
           tof = i
          elseif(pixel(j,i).EQ.'W'.AND.tof.NE.0)then
           bof = i-1
            fringe(n) = (bof+tof)/2.0
          n = n+1
           tof = 0
           bof = 0
         else
          endif
        repeat
*
*  calculation  of  d/dy
*
```

```
        n = 2
110      if(fringe(n+1).NE.0)then
             str(n) = (2.0*df*scale)/(fringe(n+1)-fringe(n-1))
           if(str(n).LT.ddymin)ddymin = str(n)
           if(str(n).GT.ddymax)ddymax = str(n)
         n = n+1
         goto 110
        else
        endif

      m = (sec*8-8)+j

      do(k=2,n-1)

           write(12,520)m,fringe(k),str(k)
        tstr = tstr + str(k)
       cnt = cnt + 1

      repeat

520   format(1x,i5,1X,f6.1,1X,e16.8)

      repeat
      width = width/8

      RETURN

      END
```

Program STRREG

```
      implicit none
      integer toolbx

      include quickdraw.inc
```

```
      include  file.inc
      include  memory.inc
      include  misc.inc
      include   utilities.inc
      include  params.inc
      include  grafport.inc

      integer  pageheight
      parameter  (pageheight=720)

*  An array to contain the bitmap data.

      integer*1  srcbits(72,  pageheight)

*  An single line of white pixels (zeros) to fill out the rest of the
*  MacPaint bitmap.

      integer*1  srcwht(72)

      integer*1  dstbuf(512)
      integer*1  grafport(grafsize)
      integer  grafptr
      integer  dstbytes

*  Pointers to the source bitmap and destination buffer.

      integer  srcptr,  dstptr
      integer  i,  j,  scanline

*  Bitmap  definitions.

      integer  bitptr
      integer*1  bitmap(14)
      integer*2  rowbytes
      integer*2  bounds(4)
      equivalence  (bitptr,  bitmap(1))
      equivalence  (rowbytes,  bitmap(5))
      equivalence  (bounds,  bitmap(7))

      character  filename*64
```

```
      integer  err

*  Rectangle for graphics operations on paint file bitmap.

      integer*2  rect(4)
      integer*1  fraction,reduction,resp,horzshft,vertshft

*  Handle to the VisRgn.

      integer  vishandle
*
*  Inputs to set region and picture scaling
*
      write(9,*)'Input the region factor,  (≥ 9)'
      read(9,*)fraction
      write(9,*)''
      write(9,*)'Input the reduction factor,  (≤ 4)'
      read(9,*)reduction
      write(9,*)''

      write(9,*)'Input the horizontal shift factor'
      read(9,*)horzshft
      write(9,*)''
      write(9,*)'Input the vertical shift factor'
      read(9,*)vertshft
      write(9,*)''

      write(9,*)'Choose the desired mapping'
      write(9,*)'1.   Axial Strains'
      write(9,*)'2.   Transverse strains'
      read(9,*)resp

      write(9,*)''
      write(9,*) 'Now creating the Strain Region MacPaint file.'

*  Initialize the bitmap buffer, grafport.

      do (i = 1, pageheight)
        do (j = 1, 72)
          srcbits(j,i) = 0
```

```
      repeat
    repeat

* Initialize the line of white pixels.

    do (i = 1, 72)
      srcwht(i) = 0
    repeat

* Initialize the grafport record.

    do (i = 1, grafsize)
      grafport(i) = 0
    repeat

    grafptr = toolbx(PTR, grafport)
    srcptr = toolbx(PTR, srcbits)
    call toolbx(OPENPORT, grafptr)

* install a pointer to the bitmap buffer.

    bitptr = srcptr

• 72 bytes per bitmap row.

    rowbytes = 72

• Bitmap bounds rectangle.

    bounds(1) = 0
    bounds(2) = 0
    bounds(3) = pageheight
    bounds(4) = 576

• Make the newly created grafport current.

    call toolbx(SETPORT, grafptr)

* Attach the newly created bitmap to the current grafport.
```

```
      call toolbx(SETPORTBITS, bitmap)

* Set the PortRect of the new grafport.

      call toolbx(PORTSIZE, 576, pageheight)

* Set the VisRgn.

      vishandle = long(grafptr + visrgn)
      call toolbx(SETRECTRGN, vishandle, 0, 0, 576, pageheight)

* Perform some graphics operations on the grafport.

      call  STRREG(fraction,reduction,resp,horzshft,vertshft)

* The grafport operations are complete.  The following code creates
a
* MacPaint file from this grafport, and requires toolbx.sub
* version 2.1 or later.


* Set the file type and owner.

      do (i = 1, 80)
        params(i) = 0
      repeat

      filename = char(6) // 'strain'
      ionameptr = toolbx(PTR, filename)

      err = toolbx(PBFILECREATE, toolbx(PTR, params))
      err = toolbx(PBGETFILEINFO, toolbx(PTR, params))
      fdtype = 'PNTG'
      fdcreator = 'MPNT'
      err = toolbx(PBSETFILEINFO, toolbx(PTR, params))

* Open the file.  Bitmap data is binary, so use unformatted access.

      open(20, file='strain', status='old',
     + form='unformatted')
```

```
* Clear out the working buffer for compressing the bitmap data.

      do (i = 1, 512)
        dstbuf(i) = 0
      repeat

* Write the MacPaint header.

      write(20)(dstbuf(i),  i=1,512)

* Get a pointer to the bitmap buffer.

      srcptr = toolbx(PTR, srcbits)

* Compress the data a scan line at a time, writting each compressed
scan
* line to the file.
*
      do (scanline = 1, pageheight)
        dstptr = toolbx(PTR, dstbuf)
        call toolbx(PACKBITS, srcptr, dstptr, 72)
        dstbytes = dstptr - toolbx(PTR, dstbuf)
        write(20)(dstbuf(i), i = 1, dstbytes)
      repeat

* Fill out the rest of the file with compressed lines of white pixels.

      srcptr = toolbx(PTR, srcwht)
      dstptr = toolbx(PTR, dstbuf)
      call toolbx(PACKBITS, srcptr, dstptr, 72)
      dstbytes = dstptr - toolbx(PTR, dstbuf)
      do (scanline = 1, 720-pageheight)
        write(20)(dstbuf(i), i = 1, dstbytes)
      repeat

      close(20)

      end
```

```
SUBROUTINE  STRREG(fraction,reduction,resp,horzshft,vertshft)

IMPLICIT NONE

INTEGER x1,y1,x2,y2,N,colm
INTEGER*4  TOOLBX,size,style,bold,normal,geneva
INTEGER*1  black(8),dk1(8),dk2(8),gray(8),ltgray(8),resp
INTEGER*1   lt1(8),lt2(8),lt3(8),white(8),fraction,reduction
INTEGER*1  horzshft,vertshft
INTEGER*2  rblack(4),rdk1(4),rdk2(4),rgray(4),rltgray(4)
INTEGER*2  rlt1(4),rlt2(4),rlt3(4),rwhite(4)
REAL  sv1,sv2,sv3,sv4,sv5,sv6,sv7,sv8,sv9,sv10
REAL  max,min,temppointy,temppointx,strain1,strain2
character*256  string


include  quickdraw.inc

black(1) = b'11111111'
black(2) = b'11111111'
black(3) = b'11111111'
black(4) = b'11111111'
black(5) = b'11111111'
black(6) = b'11111111'
black(7) = b'11111111'
black(8) = b'11111111'

dk2(1) = b'11111111'
dk2(2) = b'11111111'
dk2(3) = b'00110011'
dk2(4) = b'00110011'
dk2(5) = b'11111111'
dk2(6) = b'11111111'
dk2(7) = b'00110011'
dk2(8) = b'00110011'

dk1(1) = b'11001100'
dk1(2) = b'00110011'
dk1(3) = b'11001100'
```

```
dk1(4) = b'00110011'
dk1(5) = b'11001100'
dk1(6) = b'00110011'
dk1(7) = b'11001100'
dk1(8) = b'00110011'

gray(1) = b'11001100'
gray(2) = b'11001100'
gray(3) = b'00110011'
gray(4) = b'00110011'
gray(5) = b'11001100'
gray(6) = b'11001100'
gray(7) = b'00110011'
gray(8) = b'00110011'

ltgray(1) = b'10101010'
ltgray(2) = b'01010101'
ltgray(3) = b'10101010'
ltgray(4) = b'01010101'
ltgray(5) = b'10101010'
ltgray(6) = b'01010101'
ltgray(7) = b'10101010'
ltgray(8) = b'01010101'

lt1(1) = b'10001000'
lt1(2) = b'00100010'
lt1(3) = b'10001000'
lt1(4) = b'00100010'
lt1(5) = b'10001000'
lt1(6) = b'00100010'
lt1(7) = b'10001000'
lt1(8) = b'00100010'

lt2(1) = b'10001000'
lt2(2) = b'00000000'
lt2(3) = b'00100010'
lt2(4) = b'00000000'
lt2(5) = b'10001000'
lt2(6) = b'00000000'
lt2(7) = b'00100010'
```

```
lt2(8)  =  b'00000000'

lt3(1)  =  b'10000000'
lt3(2)  =  b'00000000'
lt3(3)  =  b'00001000'
lt3(4)  =  b'00000000'
lt3(5)  =  b'10000000'
lt3(6)  =  b'00000000'
lt3(7)  =  b'00001000'
lt3(8)  =  b'00000000'

white(1)  =  b'10000000'
white(2)  =  b'00000000'
white(3)  =  b'00001000'
white(4)  =  b'00000000'
white(5)  =  b'10000000'
white(6)  =  b'00000000'
white(7)  =  b'00001000'
white(8)  =  b'00000000'



open(unit=12,file='maxmin.out',status='old')

read(12,*)min
read(12,*)max

sv1 = min
sv2  =  sv1+(max-min)/fraction
sv3  =  sv2+(max-min)/fraction
sv4  =  sv3+(max-min)/fraction
sv5  =  sv4+(max-min)/fraction
sv6  =  sv5+(max-min)/fraction
sv7  =  sv6+(max-min)/fraction
sv8  =  sv7+(max-min)/fraction
sv9  =  sv8+(max-min)/fraction
sv10 = max

data  rlt3  /645,10,655,20/
```

```
data  rlt2  /660,10,670,20/
data  rlt1  /675,10,685,20/
data  rltgray  /690,10,700,20/
data  rgray  /645,250,655,260/
data  rdk1  /660,250,670,260/
data  rdk2  /675,250,685,260/
data  rblack  /690,250,700,260/

data geneva /3/
call toolbx(TEXTFONT,geneva)
data  bold  /1/
style = bold
call  toolbx(TEXTFACE,style)

if(resp.EQ.1)then
  string = char(23)//'AXIAL STRAIN BY REGIONS'
elseif(resp.EQ.2)then
  string = char(28)//'TRANSVERSE STRAIN BY REGIONS'
else
endif

call  toolbx(MOVETO,200,10)
call  toolbx(DRAWSTRING,string)
data  normal  /0/
style = normal
call  toolbx(TEXTFACE,style)
data  size  /9/
call  toolbx(TEXTSIZE,size)


call  toolbx(FILLRECT,rlt3,lt3)
call  toolbx(FRAMERECT,rlt3)
call  toolbx(FILLRECT,rlt2,lt2)
call  toolbx(FRAMERECT,rlt2)
call  toolbx(FILLRECT,rlt1,lt1)
call  toolbx(FRAMERECT,rlt1)
call  toolbx(FILLRECT,rltgray,ltgray)
call  toolbx(FRAMERECT,rltgray)
call  toolbx(FILLRECT,rgray,gray)
call  toolbx(FRAMERECT,rgray)
```

```
      call toolbx(FILLRECT,rdk1,dk1)
      call toolbx(FRAMERECT,rdk1)
      call toolbx(FILLRECT,rdk2,dk2)
      call toolbx(FRAMERECT,rdk2)
      call toolbx(FILLRECT,rblack,black)
      call toolbx(FRAMERECT,rblack)

      call toolbx(MOVETO,30,655)
      WRITE(*,550)sv2,sv3
      call toolbx(MOVETO,30,670)
      WRITE(*,550)sv3,sv4
      call toolbx(MOVETO,30,685)
      WRITE(*,550)sv4,sv5
      call toolbx(MOVETO,30,700)
      WRITE(*,550)sv5,sv6
      call toolbx(MOVETO,270,655)
      WRITE(*,550)sv6,sv7
      call toolbx(MOVETO,270,670)
      WRITE(*,550)sv7,sv8
      call toolbx(MOVETO,270,685)
      WRITE(*,550)sv8,sv9
      call toolbx(MOVETO,270,700)
      WRITE(*,550)sv9,sv10
550   format(1x,'strain = ',e10.4,' to ',e10.4)

      if(resp.EQ.1)then
         open(unit=11,file='ddy.output',status='old')
      elseif(resp.EQ.2)then
         open(unit=11,file='ddx.output',status='old')
      else
      endif

      if(resp.EQ.1)then
         read(11,*,end=600,ERR=600)x1,temppointy,strain1
        y1 = ifix(temppointy)
      elseif(resp.EQ.2)then
         read(11,*,end=600,ERR=600)temppointx,y1,strain1
        x1 = ifix(temppointx)
      else
      endif
```

```
      x1  =  ifix(x1/reduction)  -  horzshft
      y1  =  ifix(y1/reduction)  +  vertshft

      if(resp.EQ.1)then
         read(11,*,end=600,ERR=600)x2,temppointy,strain2
        y2  =  ifix(temppointy)
      elseif(resp.EQ.2)then
         read(11,*,end=600,ERR=600)temppointx,y2,strain2
        x2  =  ifix(temppointx)
      else
      endif

      x2  =  ifix(x2/reduction)  -  horzshft
      y2  =  ifix(y2/reduction)  +  vertshft


400   if(strain1.GE.sv1.AND.strain1.LT.sv2)then
       CALL TOOLBX(PENPAT,white)
      elseif(strain1.GE.sv2.AND.strain1.LT.sv3)then
       CALL TOOLBX(PENPAT,lt3)
      elseif(strain1.GE.sv3.AND.strain1.LT.sv4)then
       CALL TOOLBX(PENPAT,lt2)
      elseif(strain1.GE.sv4.AND.strain1.LT.sv5)then
       CALL TOOLBX(PENPAT,lt1)
      elseif(strain1.GE.sv5.AND.strain1.LT.sv6)then
       CALL TOOLBX(PENPAT,ltgray)
      elseif(strain1.GE.sv6.AND.strain1.LT.sv7)then
       CALL TOOLBX(PENPAT,gray)
      elseif(strain1.GE.sv7.AND.strain1.LT.sv8)then
       CALL TOOLBX(PENPAT,dk1)
      elseif(strain1.GE.sv8.AND.strain1.LT.sv9)then
       CALL TOOLBX(PENPAT,dk2)
      else
       CALL TOOLBX(PENPAT,black)
      endif

        CALL TOOLBX(MOVETO,x1,y1)
        CALL TOOLBX(LINETO,x2,y2)
```

```
x1 = x2
y1 = y2
strain1 = strain2

if(resp.EQ.1)then
   read(11,*,end=600,ERR=600)x2,temppointy,strain2
  y2 = ifix(temppointy)
elseif(resp.EQ.2)then
   read(11,*,end=600,ERR=600)temppointx,y2,strain2
  x2 = ifix(temppointx)
else
endif

x2 = ifix(x2/reduction) - horzshft
y2 = ifix(y2/reduction) + vertshft

if(resp.EQ.1)then

if(x1.NE.x2)then
  x1 = x2
  y1 = y2
   strain1 = strain2

if(resp.EQ.1)then
   read(11,*,end=600,ERR=600)x2,temppointy,strain2
  y2 = ifix(temppointy)
elseif(resp.EQ.2)then
   read(11,*,end=600,ERR=600)temppointx,y2,strain2
  x2 = ifix(temppointx)
else
endif

x2 = ifix(x2/reduction) - horzshft
y2 = ifix(y2/reduction) + vertshft

else
endif

elseif(resp.EQ.2)then
```

```
      if(y1.NE.y2)then
        x1 = x2
        y1 = y2
         strain1 = strain2

      if(resp.EQ.1)then
         read(11,*,end=600,ERR=600)x2,temppointy,strain2
        y2 = ifix(temppointy)
      elseif(resp.EQ.2)then
         read(11,*,end=600,ERR=600)temppointx,y2,strain2
        x2 = ifix(temppointx)
      else
      endif

      x2 = ifix(x2/reduction) - horzshft
      y2 = ifix(y2/reduction) + vertshft

      else
      endif

      else
      endif


      goto 400

600   RETURN
      END
```